Supplementary Information

Light-induced selectivity in an exemplary photodimerization reaction of varied azaanthracenes.

Adam Mames,[a] Aleksander Gorski, [a] Joanna Jankowska,[b] Tomasz Ratajczyk*, [a] Mariusz Pietrzak*[a]

[a] Institute of Physical Chemistry, Polish Academy of Sciences, Kasprzaka 44/52, 01- 224 Warsaw, Poland, tratajczyk@ichf.edu.pl, mpietrzak@ichf.edu.pl,
[b] Faculty of Chemistry, University of Warsaw, Pasteura 1, 02-093 Warsaw, Poland

List of contents

1.General information

All NMR spectra were acquired on a Bruker AVANCE II 300 MHz spectrometer equipped with a BBI W1 5 mm Z-gradient probe. The temperature was controlled by a BVT-3000 unit. The spectrometer was operated by the TOPSPIN 2.0 program.

Materials

All commercially available chemicals for synthesis were bought from Sigma-Aldrich or TCI Chemicals and used without any further purification. All NMR solvents were purchased from EUROISOTOP and used as obtained.

Sample preparation

Synthesis: 2-Azaanthracene (**A**) and N-methyl-2-azaantracene (**M**) iodide were synthesized according to the literature.[1] The ^{1}H, ^{13}C NMR, as well as ^{1}H-NOESY, ^{1}H-COSY and ^{1}H-^{13}C HSQC spectra of pure **A** and **M** are available in the Supporting Information.

NMR Samples and Measurements. Deuterated CD_3OD and CD_2Cl_2 in 0.75 ml ampules were obtained from Deutero GmbH (99.6% D) and were used without further purification. Sample concentrations were about 1-2 mM. Samples were prepared in contact with atmospheric air, and therefore they contained dissolved air. Degassed samples were obtained by a cool-pump-thaw procedure repeated 3 times in tight sealed NMR tubes with the septum.

NMR spectra were acquired on two spectrometers: a Bruker AVANCE II 300 MHz with a WB magnet equipped with a 5 mm BBI Z-gradient probe head, and on a Bruker AVANCE II 500 MHz spectrometer with a WB magnet equipped with a 5 mm BBO Z-gradient probe. The temperature was controlled by a BVT-3000 unit. The spectrometers were operated via the TOPSPIN program (version 2.0 at 500 MHz and 3.2 at 300 MHz). The NOESY (mixing time 1.2 s), COSY and HSQC experiments were performed with standard Bruker pulse programs (noesygpph, cosygpmfph, hsqcgpph). The reference for ^{1}H NMR was the signal of CHD_2OD and $CHDCl_2$ set to 3.32 and 5.32 ppm, respectively.

Simulation of multiplets was performed with DAISY Spectrum Simulation Module (version 3.5.2) built in Topsin 4.0.7.

Irradiation. The irradiation was realized with a UV-diode emitting at 365 nm (Thorlabs M365LP1-C4), at 420 nm (Thorlabs M420L3). The irradiation outside the magnet was done directly in an NMR tube through the glass (it was checked that the transmittance of light at 365 nm was above 95%, roughly estimated light beam power delivered to the sample was about 20 mW).
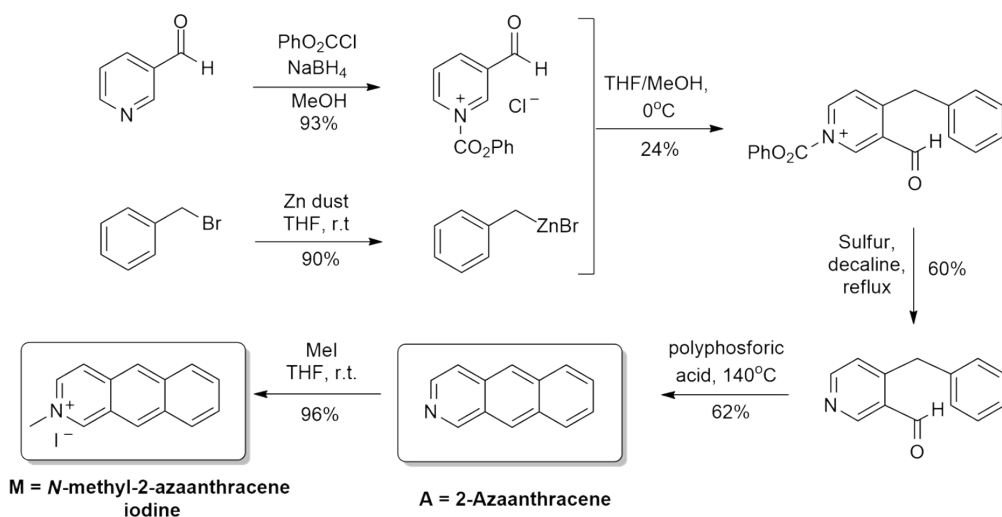
Fig. S1. The synthetic route to 2-Azaanthracene (**A**) and N-Me-2-azaanthracene (**M**) according to the literature available procedures.[1]
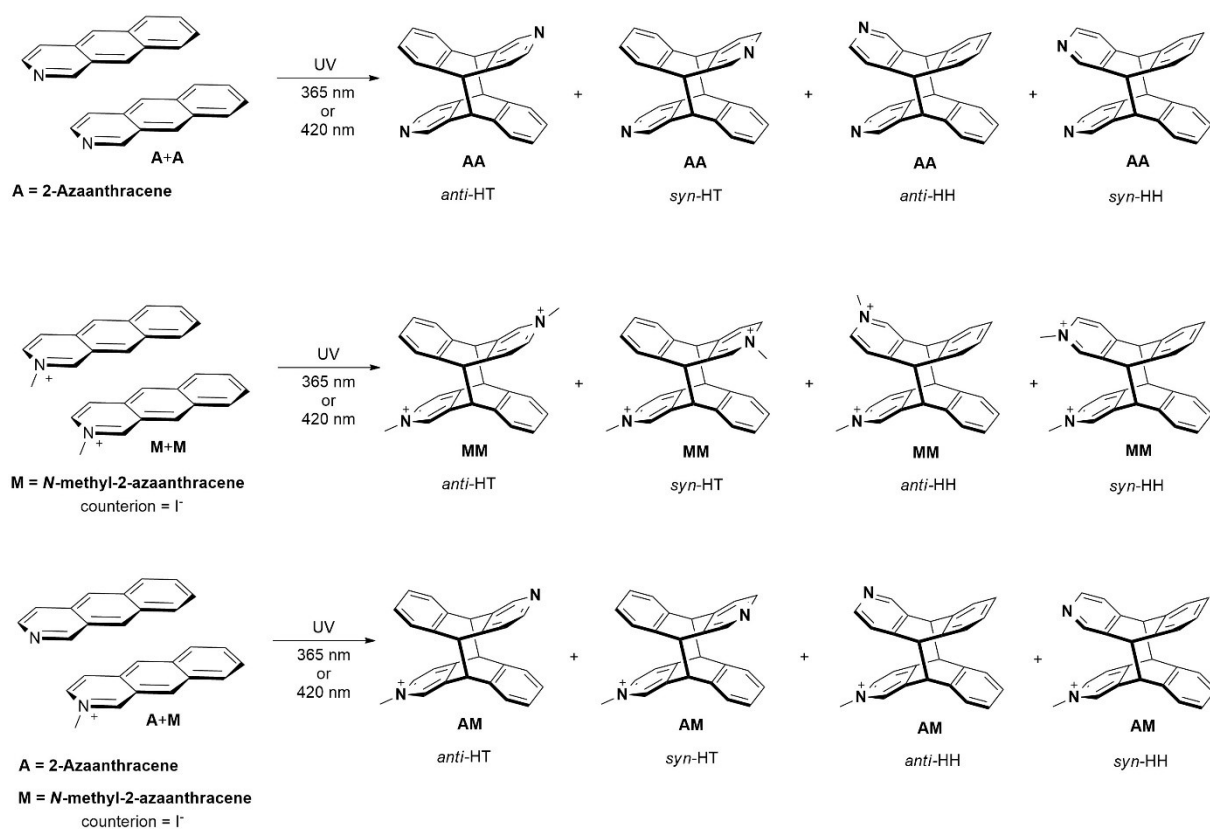

Fig. S2. Possible photodimers of the photoreaction in the mixture of 2-Azaanthracene (**A**) and N-Methyl-2-azaanthracene (**M**).

Electronic absorption

The electronic absorption measurements were carried out on Shimadzu 2700 absorption spectrophotometer. Spectral grade toluene and dichloromethane (for spectroscopy Uvasol, Merck) were used to prepare all the solutions.

Determination of photodegradation quantum yield.

The azaanthracene derivatives dissolved in methanol or dichloromethane, placed in a sealed quartz cuvette, were irradiated with light emitted by LED diodes (λ = 365 or 420 nm). High power LEDs (Thorlabs M420L3 and M365L) were used for irradiation. The light intensity was determined by power meter as 102 and 170 mW for 365 nm and 420 nm LEDs, respectively. The sample solutions were stirred during the irradiation. The photodegradation process was monitored by UV-vis absorption measurements (Shimadzu UV2700). The photodegradation quantum yield was determined by measuring the sample absorbance before irradiation (A_0) and at time t after the beginning of irradiation ($A(t)$). Next the $A_0/A(t)$ ratio was plotted as a function of $F(t)$, defined as $N_{tot}(t)/A(t)$, where $N_{tot}(t)$ denotes the total number of photons absorbed after irradiating the sample for time t. The photodegradation quantum yield was calculated based on following equation: $\Phi_{pho} = (b \times N_{Av} \times V)/(1000 \times \varepsilon \times l)$; where b is the slope in the equation: $A_0/A(t) = 1 + bF(t)$, N_{Av} is the Avogadro number, V is the sample volume (in mL), ε is the molar absorption coefficient at the wavelength selected to monitor absorbance decrease, and l is the optical path length (in cm). The detailed procedure of the determination and calculation of the quantum yield of photodegradation is described elsewhere [2].
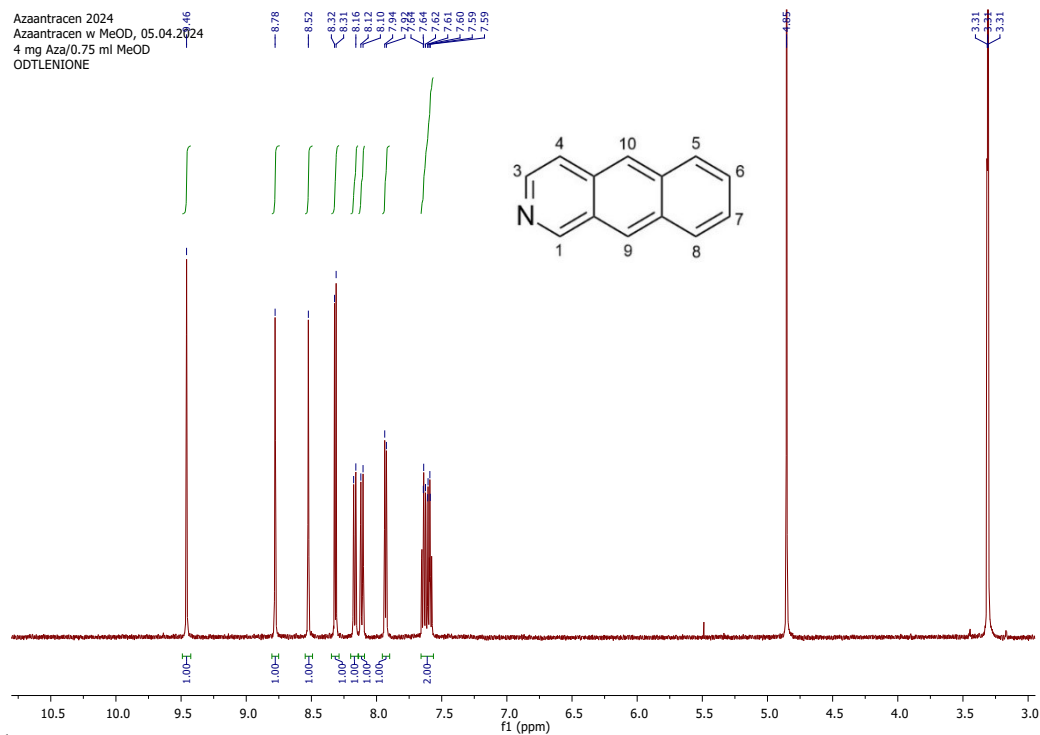
2. NMR spectra

Substrates (A and M)

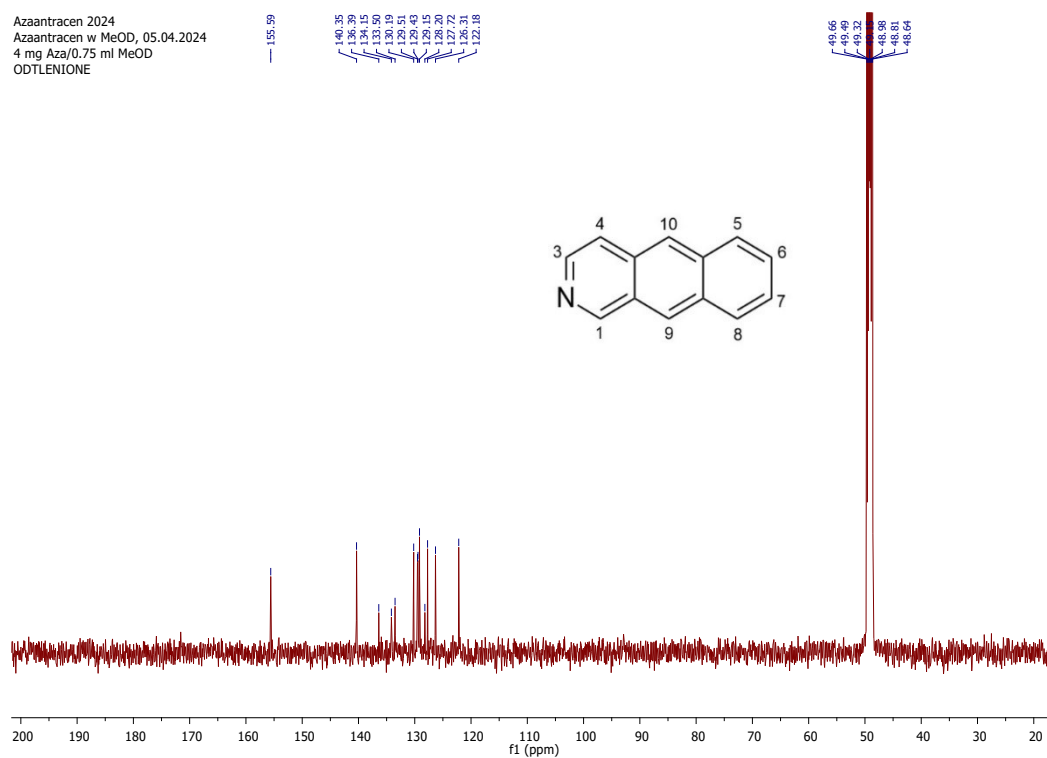Fig. S3. ^{1}H NMR of 2-Azaanthracene (**A**) in methanol-d_4 measured at 500 MHz at 298 K.

Fig. S4. ^{13}C NMR of 2-Azaanthracene (**A**) in methanol-d_4 measured at 500 MHz at 298 K.
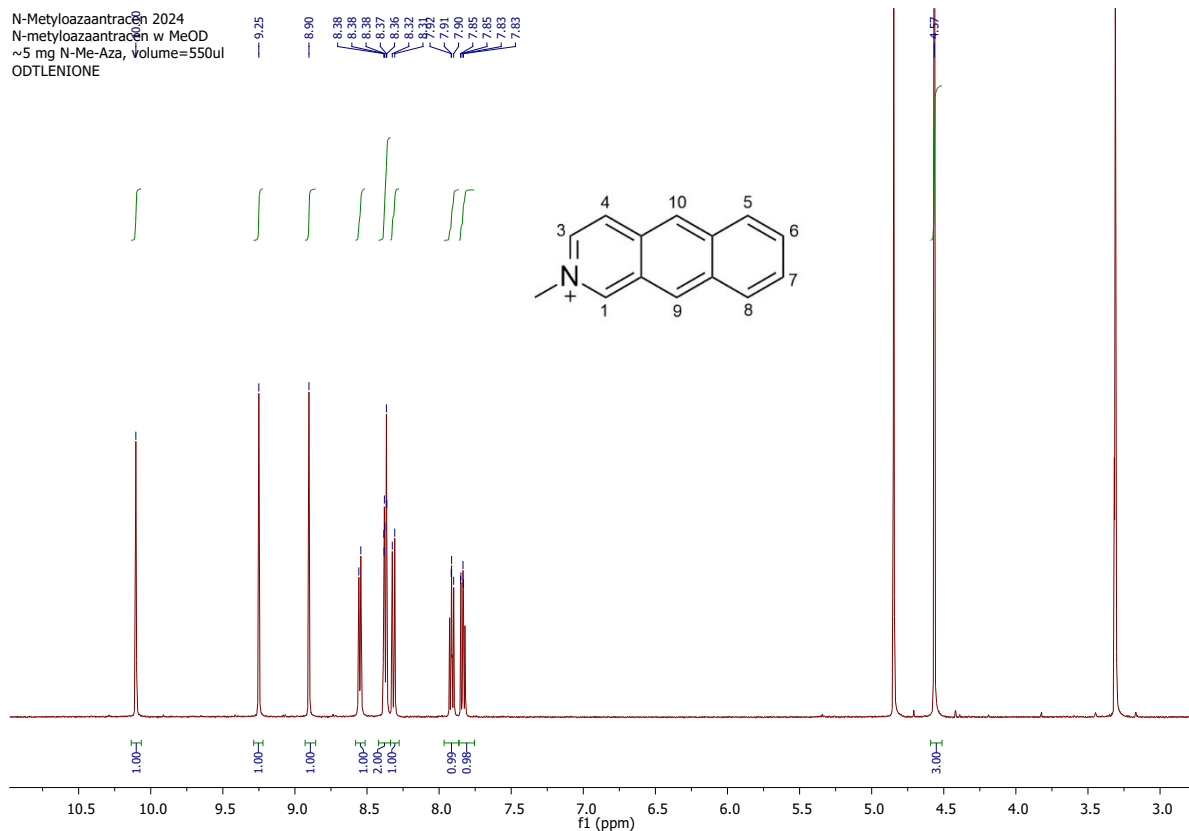
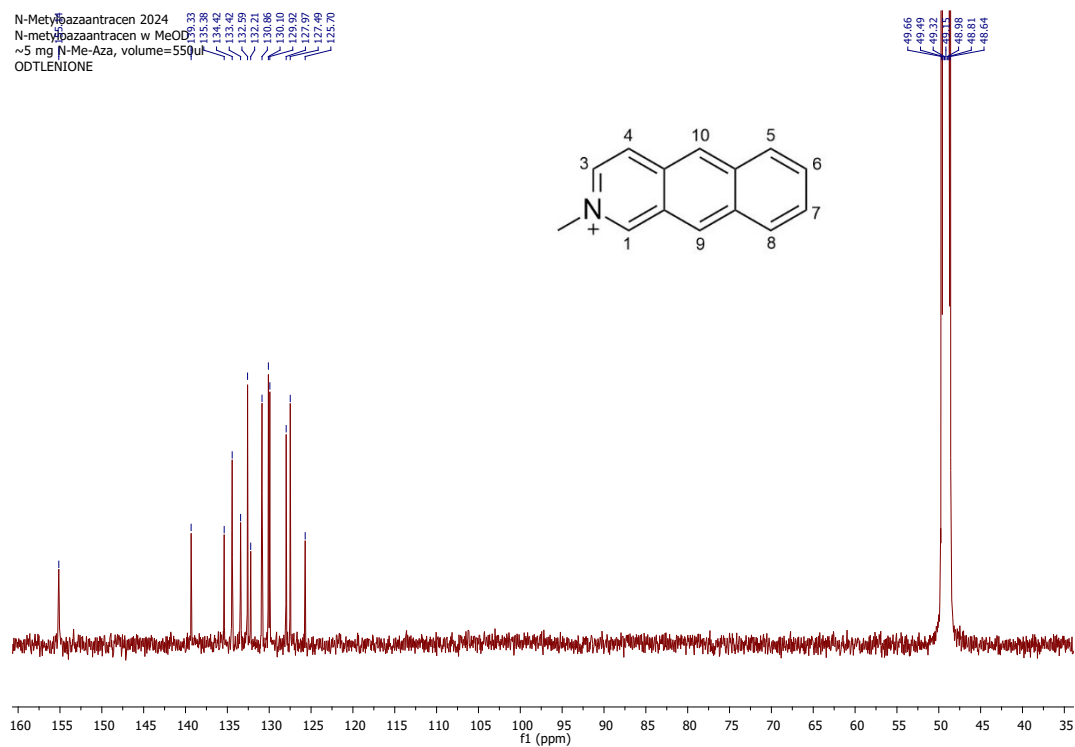Fig. S5. ^{1}H NMR of N-Me-2-azaanthracene (**M**) in methanol-d_4 measured at 500 MHz at 298 K.

Fig. S6. ^{13}C NMR of N-Me-2-azaanthracene (**M**) in methanol-d_4 measured at 500 MHz at 298 K.
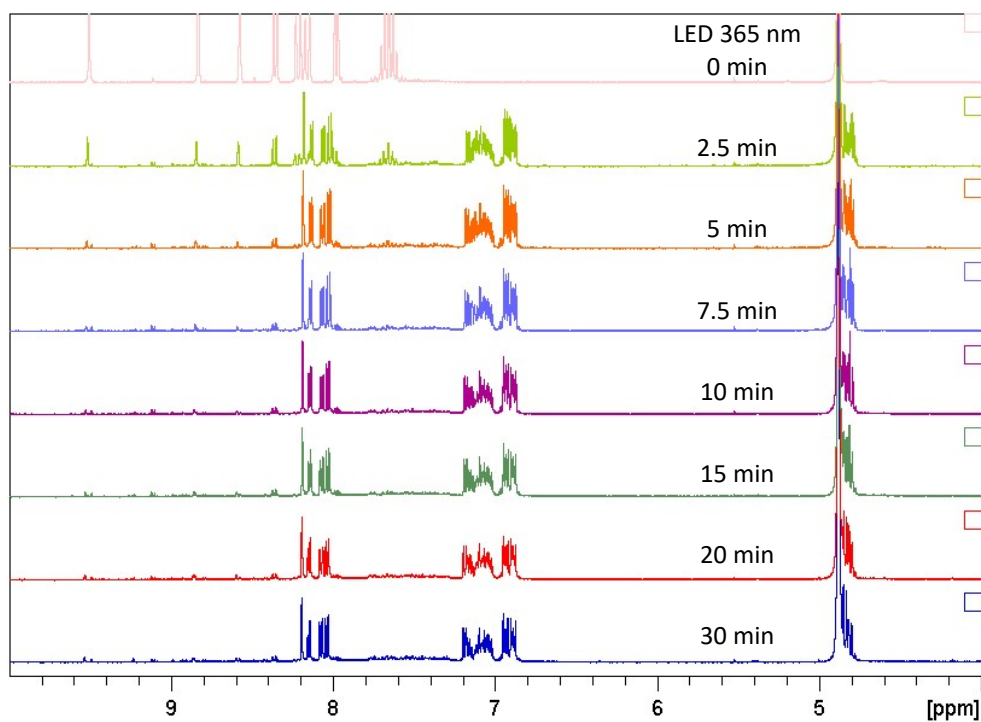
Irradiation of A

Fig. S7. ^{1}H NMR spectra recorded during irradiation of 2-Azaanthracene (**A**) in methanol-d_4 at 365 nm measured at 300 MHz at 298 K. Four different regiomers **AA** were formed.
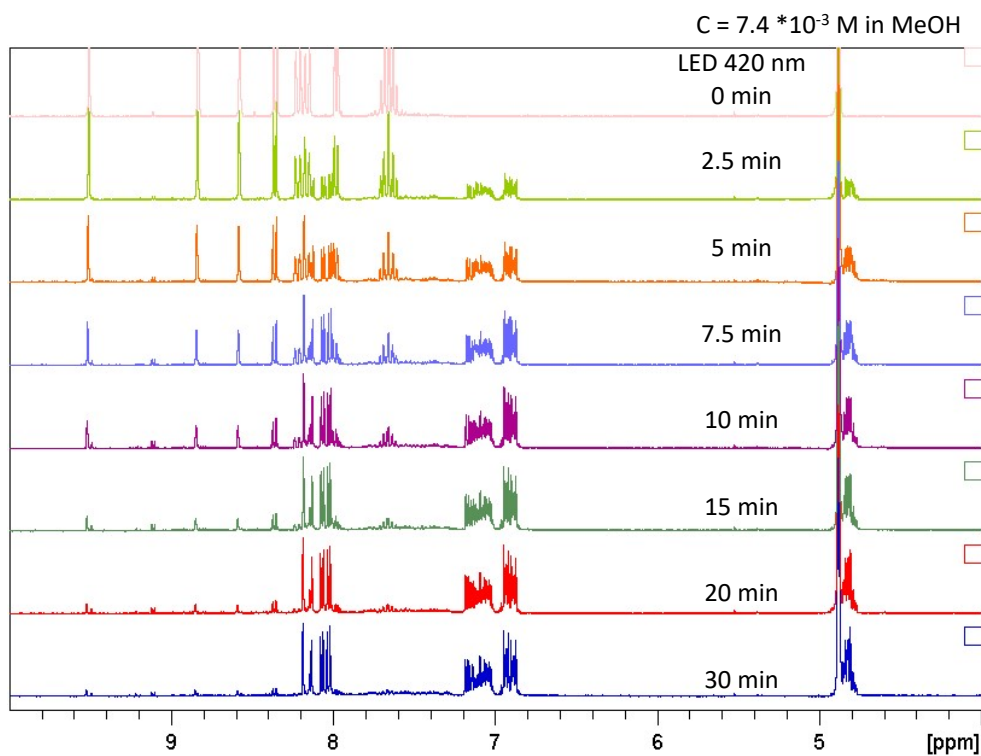

Fig. S8. ^{1}H NMR spectra recorded during irradiation of 2-azaanthracene (**A**) in methanol-d_4 at 420 nm measured at 300 MHz at 298 K. Four different regiomers **AA** were formed.
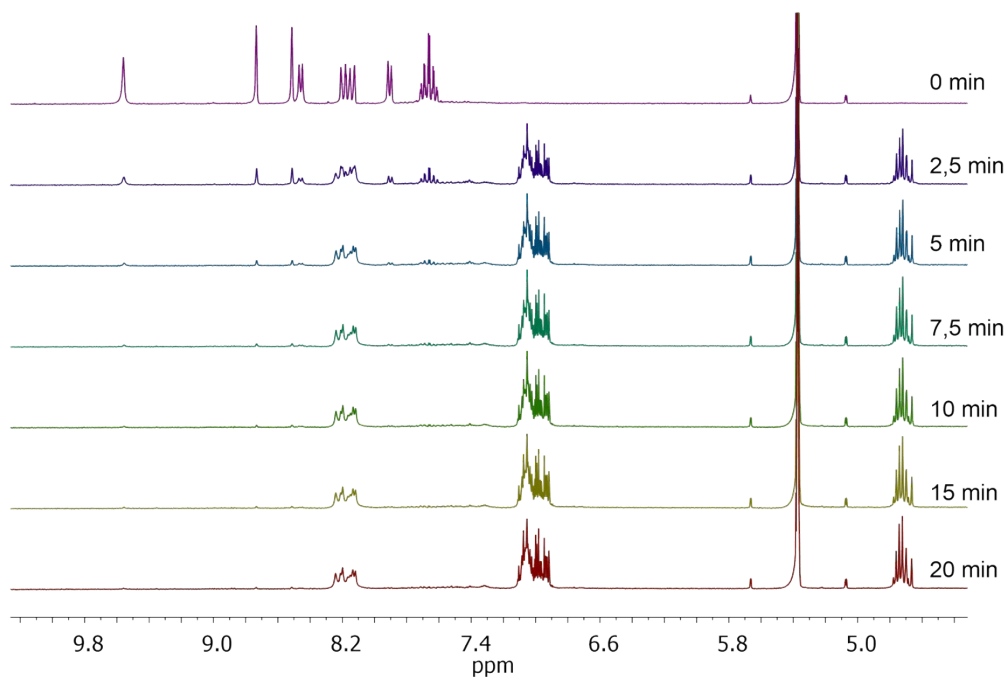
Fig. S9. ^{1}H NMR spectra recorded during irradiation of 2-azaanthracene (**A**) in CD$_2$Cl$_2$ at 365 nm measured at 300 MHz at 298 K.
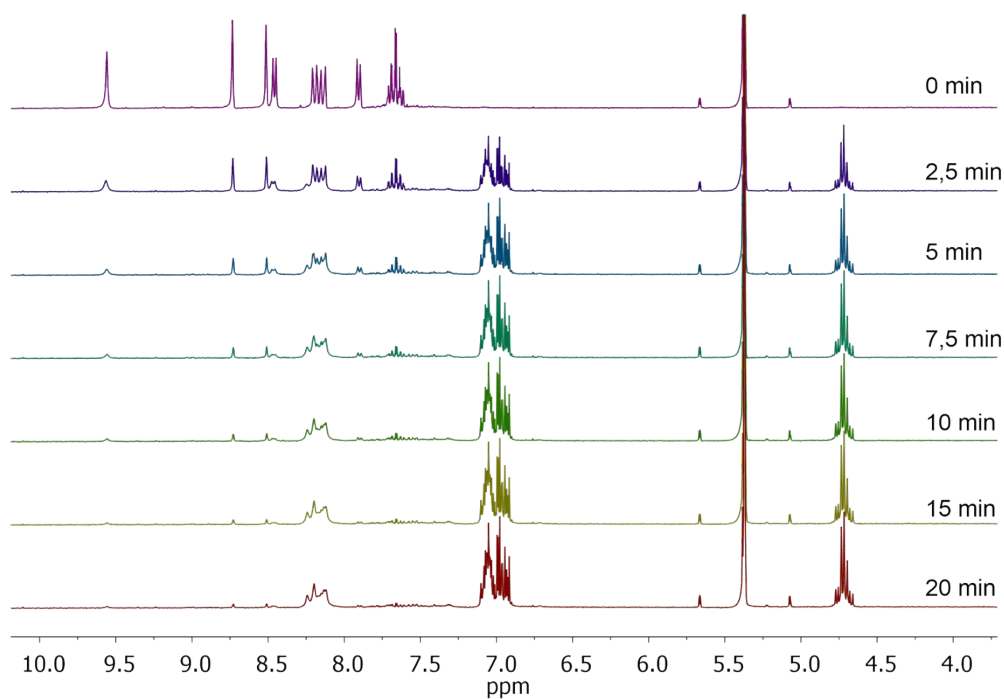

Fig. S10. ^{1}H NMR spectra recorded during irradiation of 2-azaanthracene (**A**) in CD$_2$Cl$_2$ at 420 nm measured at 300 MHz at 298 K.
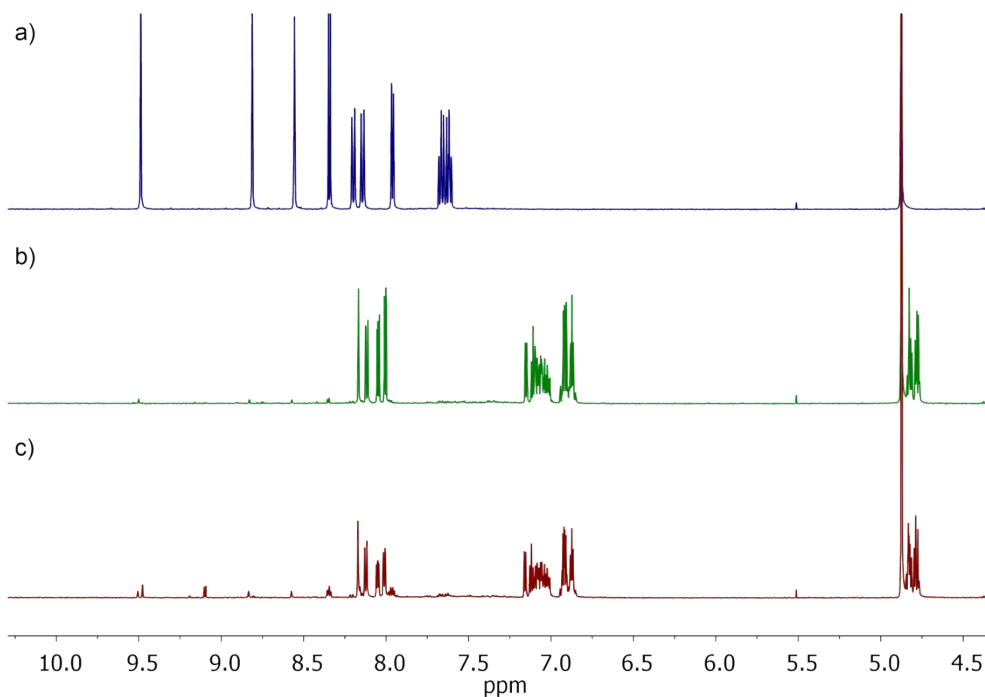
Fig. S11. ¹H NMR spectra recorded: a) before irradiation of 2-azaanthracene (**A**) in methanol-d_4 b) after 10 min irradiation at 365 nm measured at 500 MHz at 298 K without oxygen. c) after 10 min irradiation at 365 nm measured at 500 MHz at 298 K with oxygen.
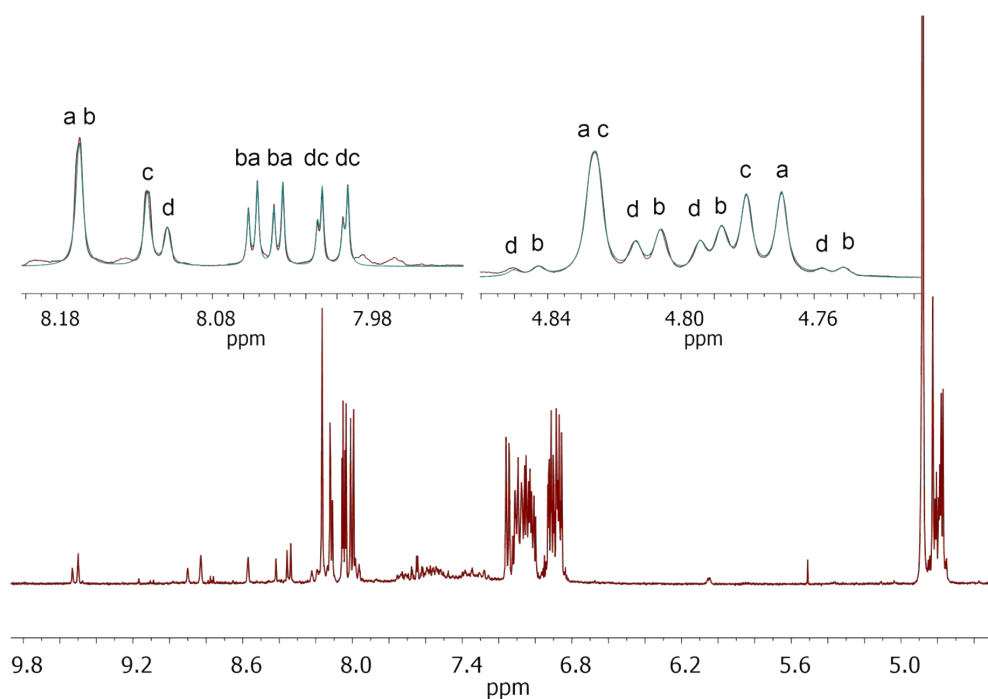

Fig. S12. ¹H NMR spectrum recorded after 10 min of irradiation at 365 nm of 2-azaanthracene (**A**) in methanol-d_4 measured at 300 MHz at 298 K after keeping at 273 K in dark for a night. The inserts show two essential regions of the spectrum (red) together with simulations of signals from four **AA** regiomers (blue) – b,d-*anti*, a,c-*syn*, b:a:d:c = 22:33:15:30
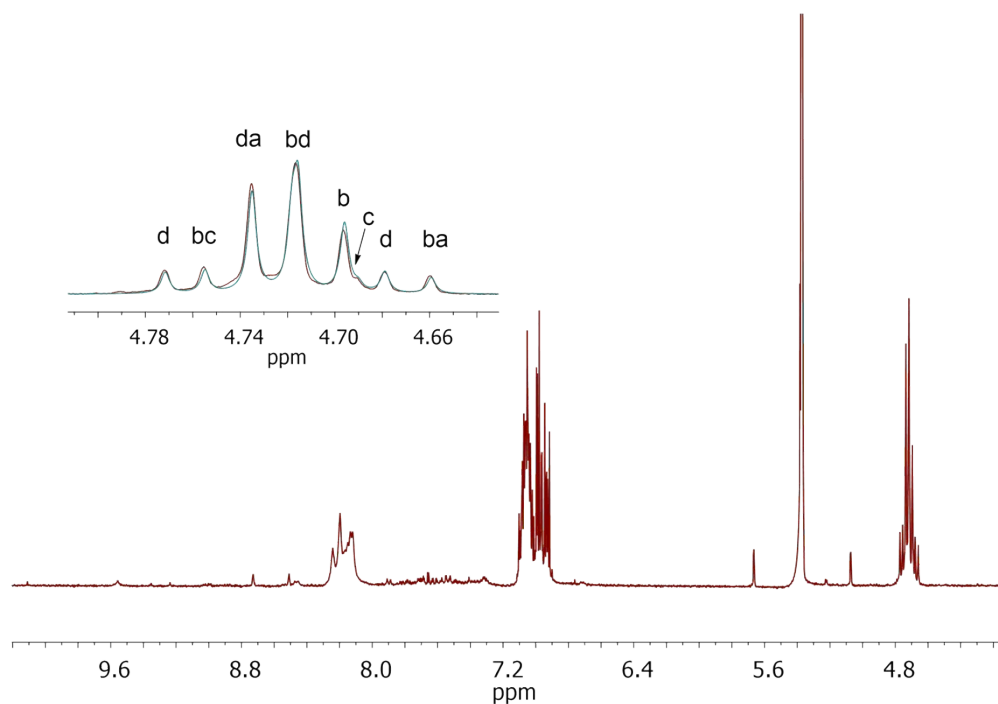
Fig. S13. ^{1}H NMR spectrum recorded after 20 min of irradiation at 420 nm of 2-azaanthracene (**A**) in CD$_2$Cl$_2$ measured at 300 MHz at 298 K. The insert shows an essential region of the spectrum (red) together with simulations of lines from four **AA** regiomers (blue) - b,d-*anti*, a,c-*syn*, b:a:d:c = 35:2:59:4.

Fig. S14. ^{1}H NMR spectrum recorded after 20 min of irradiation at 365 nm of 2-azaanthracene (**A**) in CD$_2$Cl$_2$ measured at 300 MHz at 298 K. The insert shows an essential region of the spectrum (red) together with simulations of lines from four **AA** regiomers (blue) - – b,d-*anti*, a,c-*syn*, b:a:d:c = 27:15:39:19
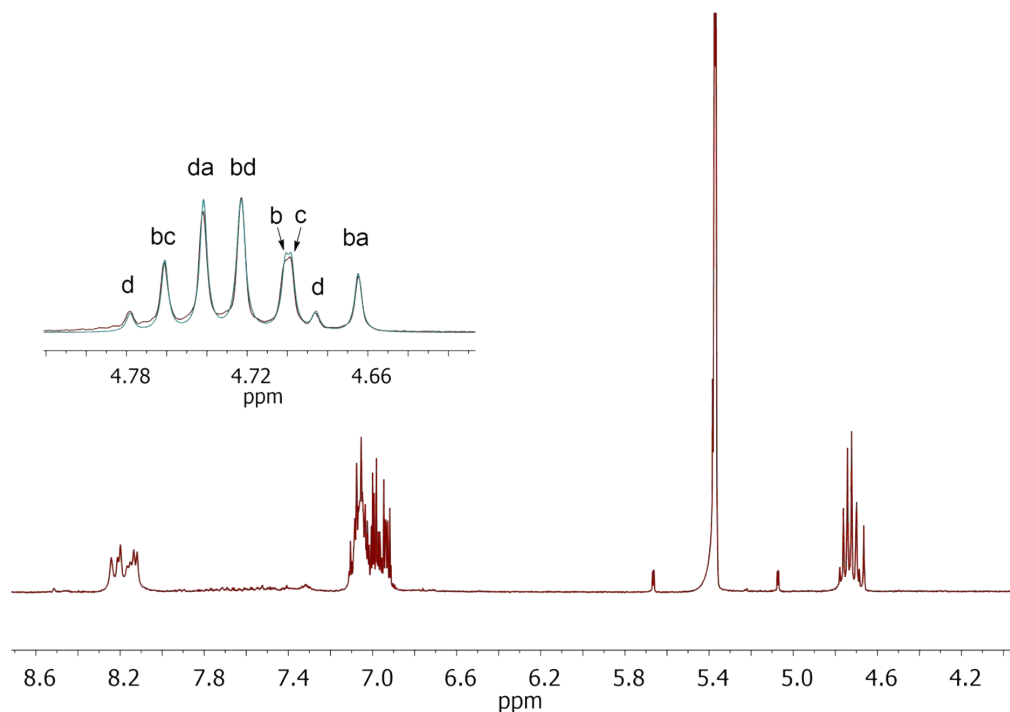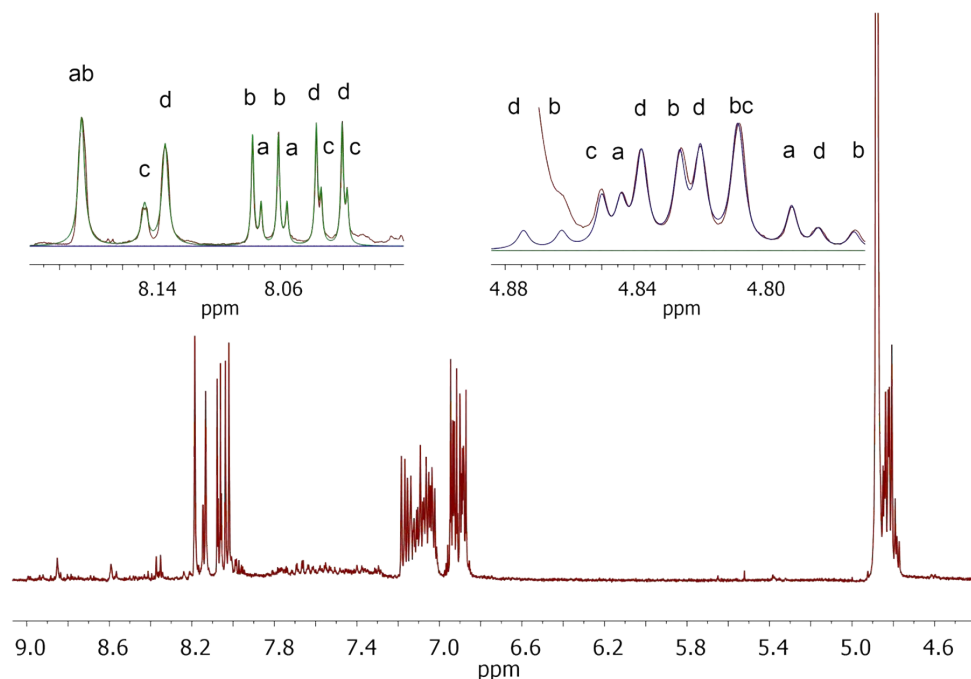
Fig. S15. ¹H NMR spectrum recorded after 30 min of irradiation at 420 nm of 2-azaanthracene (**A**) in methanol-d_4 measured at 300 MHz at 298 K. The inserts show two essential regions of the spectrum (red) together with simulations of lines from four **AA** regiomers (blue and green) – b,d-*anti*, a,c-*syn*, b:a:d:c = 35:13:37:15.

Fig. S16. ¹H NMR spectrum recorded after 20 hours of irradiation at 365 nm of 2-azaanthracene (**A**) in methanol-d_4 measured at 300 MHz at 298 K. The inserts show two essential regions of the spectrum (red) together with simulations of lines from four **AA** regiomers (blue and green) – b,d-*anti*, a,c-*syn*, b:a:d:c = 35:21:31:13..
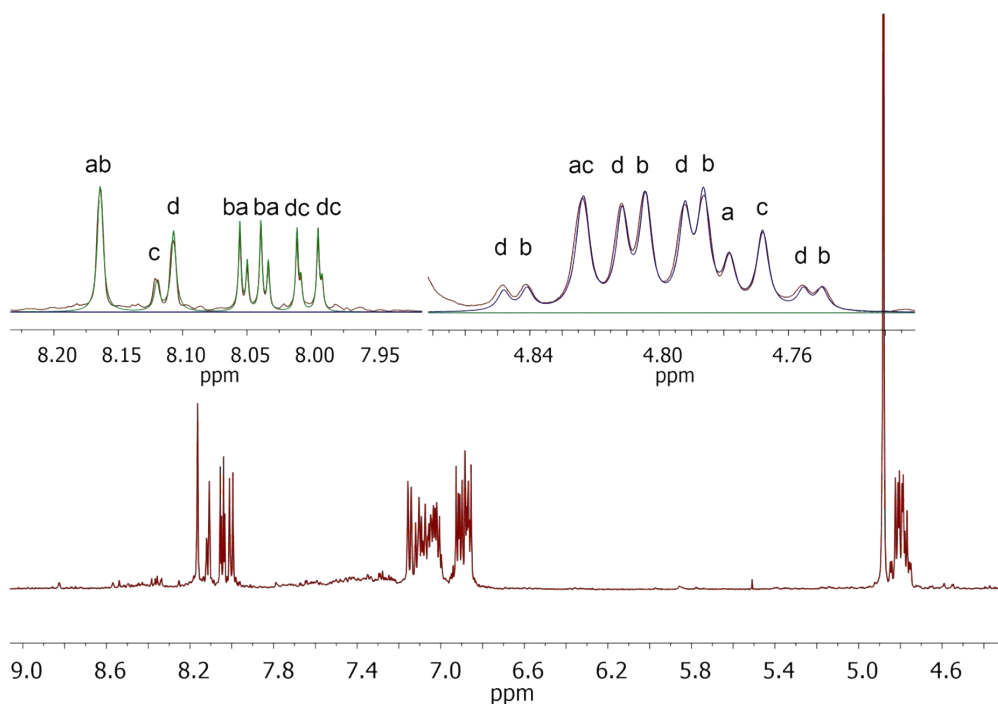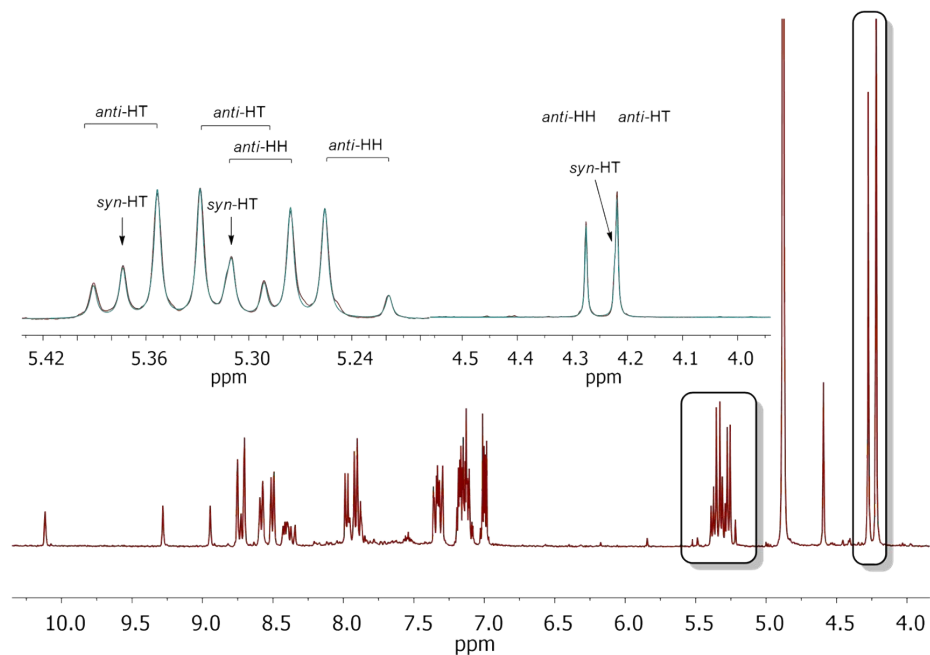
Irradiation of M

Fig. S17. ^{1}H NMR spectrum of N-methyl-2-azaanthracene (**M**) iodide after 60 min of irradiation at 420 nm in methanol-d_4 measured at 300 MHz at 298 K. The initial concentration of **M** was 4.7 * 10^{-3} M. The inserts show H9, H10 and Me signals (red) together with simulations of lines for three **MM** regiomers (blue): *anti*-HT : *anti*-HH : *syn*-HT = 47 : 38 : 14.

Fig. S18. ^{1}H NMR spectrum of N-methyl-2-azaanthracene (**M**) iodide after 8 hours of irradiation at 420 nm at lower power in methanol-d_4 measured at 500 MHz at 298 K. The initial concentration of **M** was higher, i.e., 1.3 * 10^{-2} M. The inserts show H9, H10 and Me signals (red) together with simulations of lines for three **MM** regiomers (blue): *anti*-HT : *anti*-HH : *syn*-HT = 51 : 41 : 8.
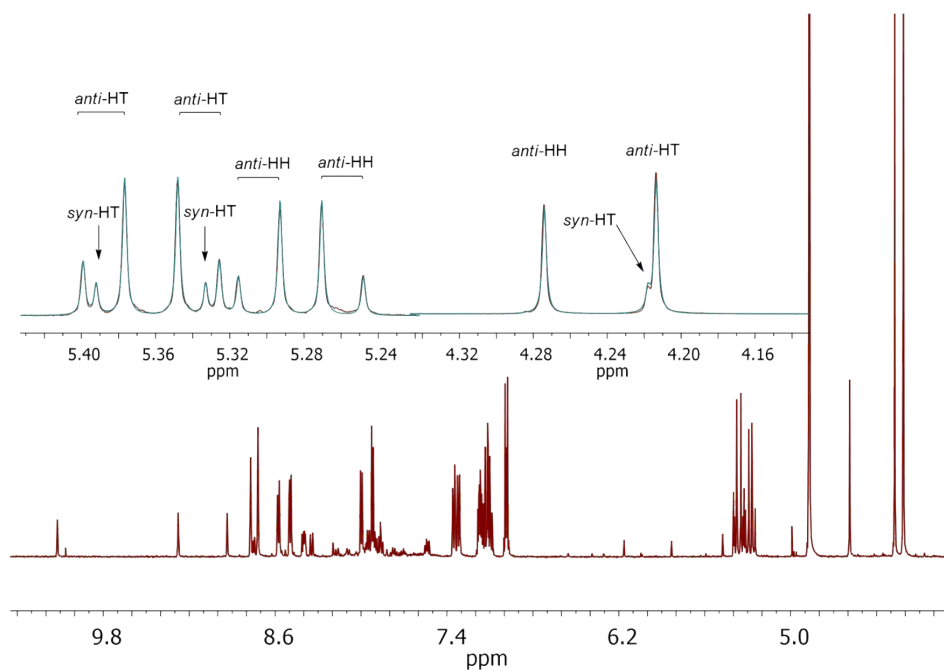
Fig. S19. ^{1}H-^{1}H COSY spectrum of N-methyl-2-azaanthracene (**M**) after irradiation at 420 nm in methanol-d_4 measured at 500 MHz at 298 K.

Fig. S20. ^{1}H-^{13}C HSQC spectrum of N-methyl-2-azaanthracene (**M**) after irradiation at 420 nm in methanol-d_4 measured at 500 MHz at 298 K. The ^{1}H region between 5.43 and 5.23 ppm is depicted showing signals of H9 and H10. Two strongly coupled doublets stand for *anti*-HT and *anti*-HH isomers, whereas two singlets labeled with red circles may be assigned to *syn*-HT isomer.

Fig. S21. ^{1}H-^{13}C HSQC spectrum of N-methyl-2-azaanthracene (**M**) and after irradiation at 420 nm in methanol-d_4 measured at 500 MHz at 298 K. The ^{1}H region between 4.31 and 4.19 ppm is depicted showing signals N-methyl. Two strong singlets stand for *anti*-HT and *anti*-HH isomers, whereas additional weak cross-peak may be assigned to traces of the *syn*-HT isomer.
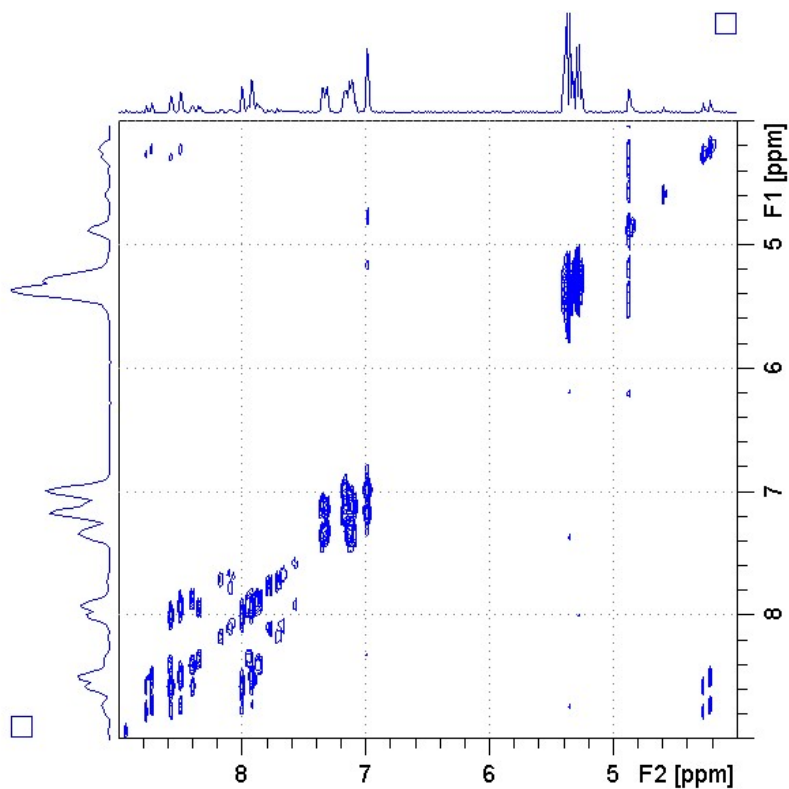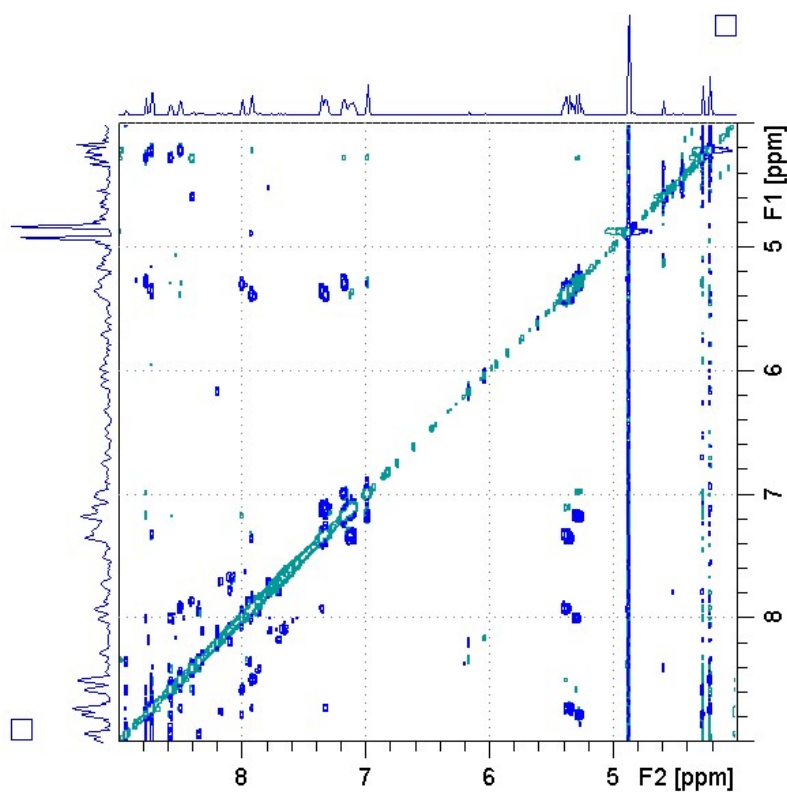

Fig. S22. ^{1}H-^{1}H NOESY spectrum of N-methyl-2-azaanthracene (**M**) after irradiation at 420 nm in methanol-d_4 measured at 500 MHz at 298 K. Mixing time was 1.2 s.
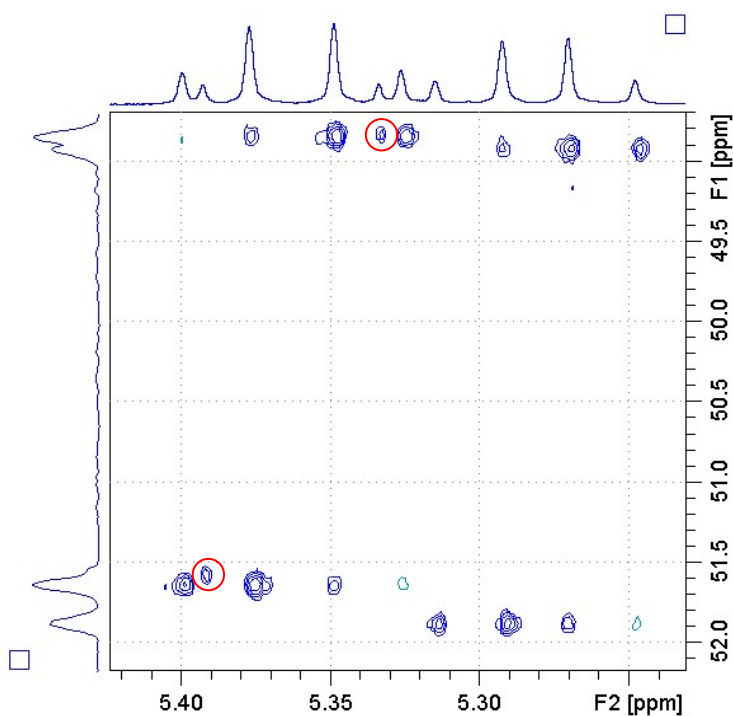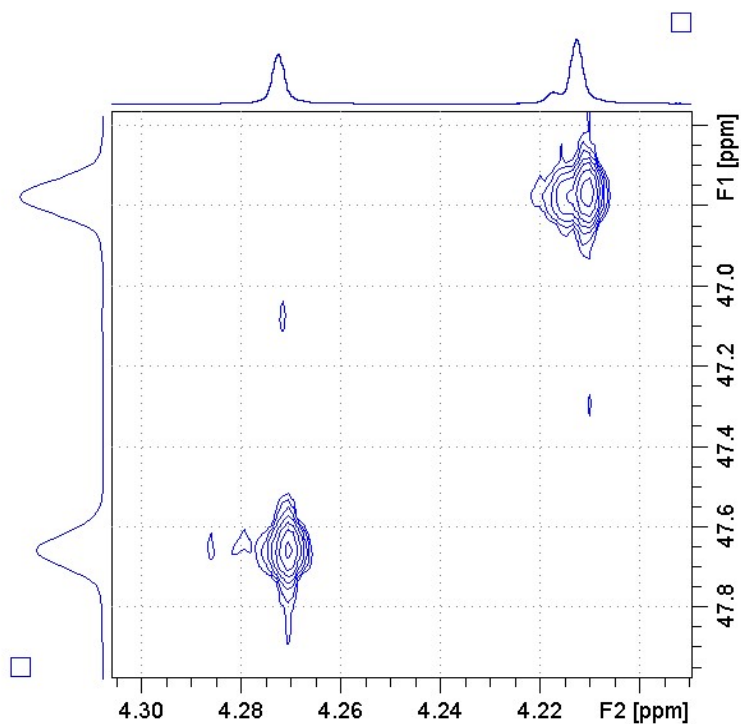
Irradiation of A + M
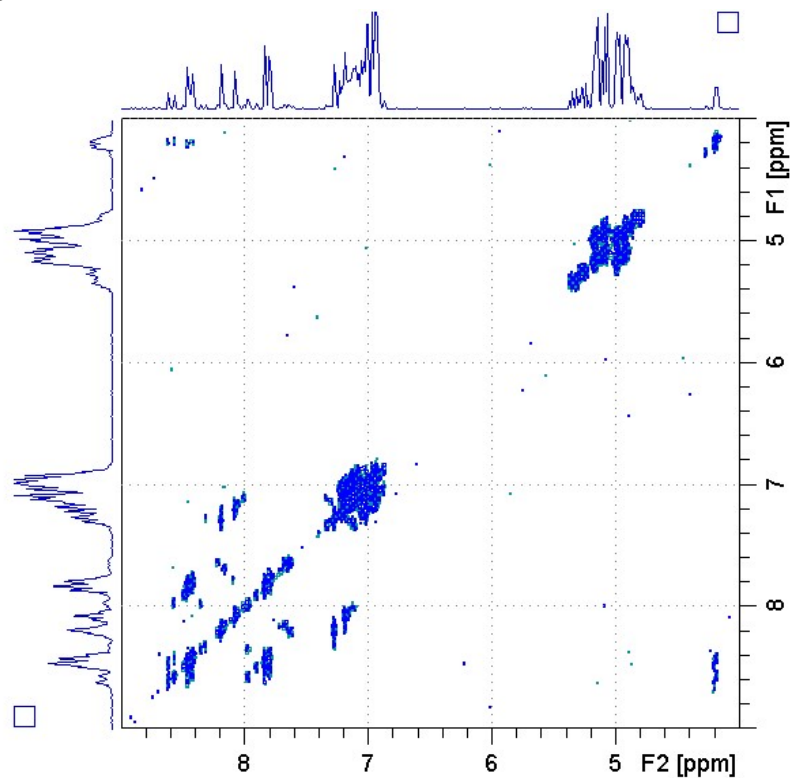
Fig. S23. ^{1}H-^{1}H COSY spectrum of the 1:1 mixture of 2-azaanthracene (**A**) and N-methyl-2-azaanthracene (**M**) after irradiation at 420 nm in methanol-d_4 measured at 500 MHz at 298 K.
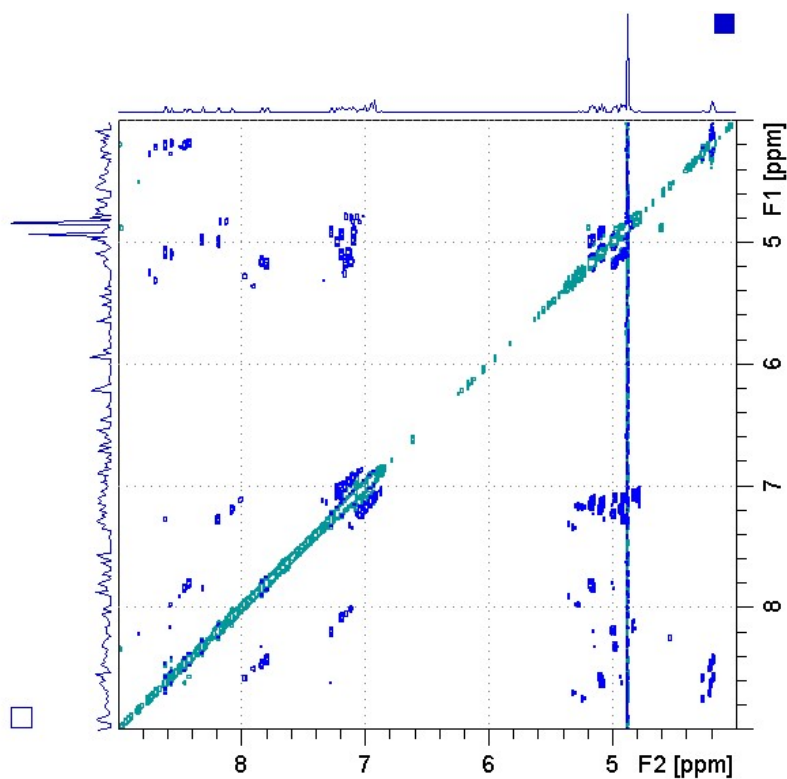
Fig. S24. ^{1}H-^{1}H NOESY spectrum of the 1:1 mixture of 2-azaanthracene (**A**) and N-methyl-2-azaanthracene (**M**) after irradiation at 420 nm in methanol-d_4 measured at 500 MHz at 298 K. Mixing time was 1.2 s.
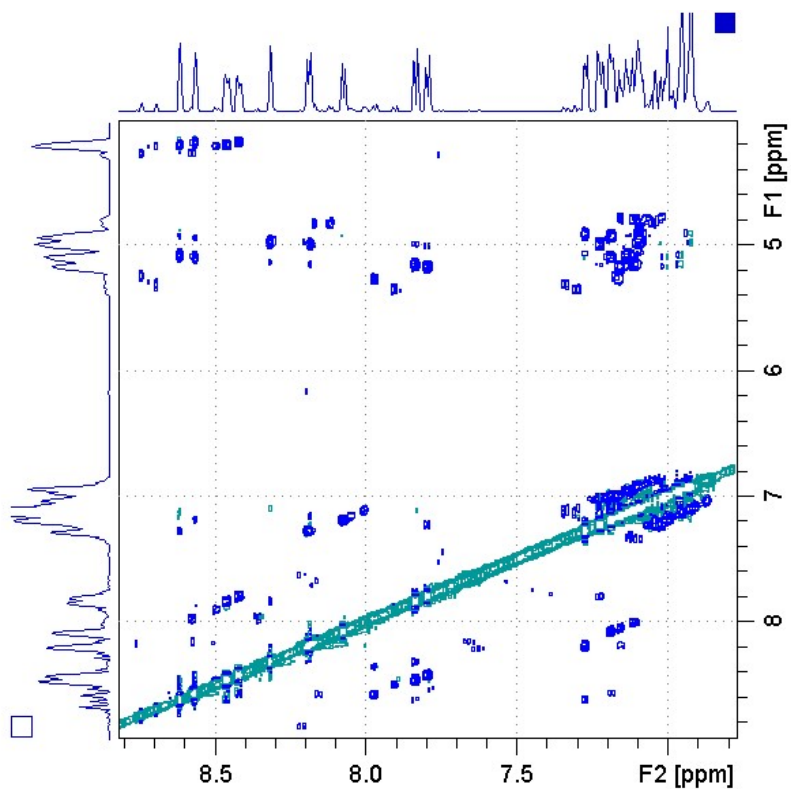
Fig. S25. Part of the spectrum from Fig. S24.
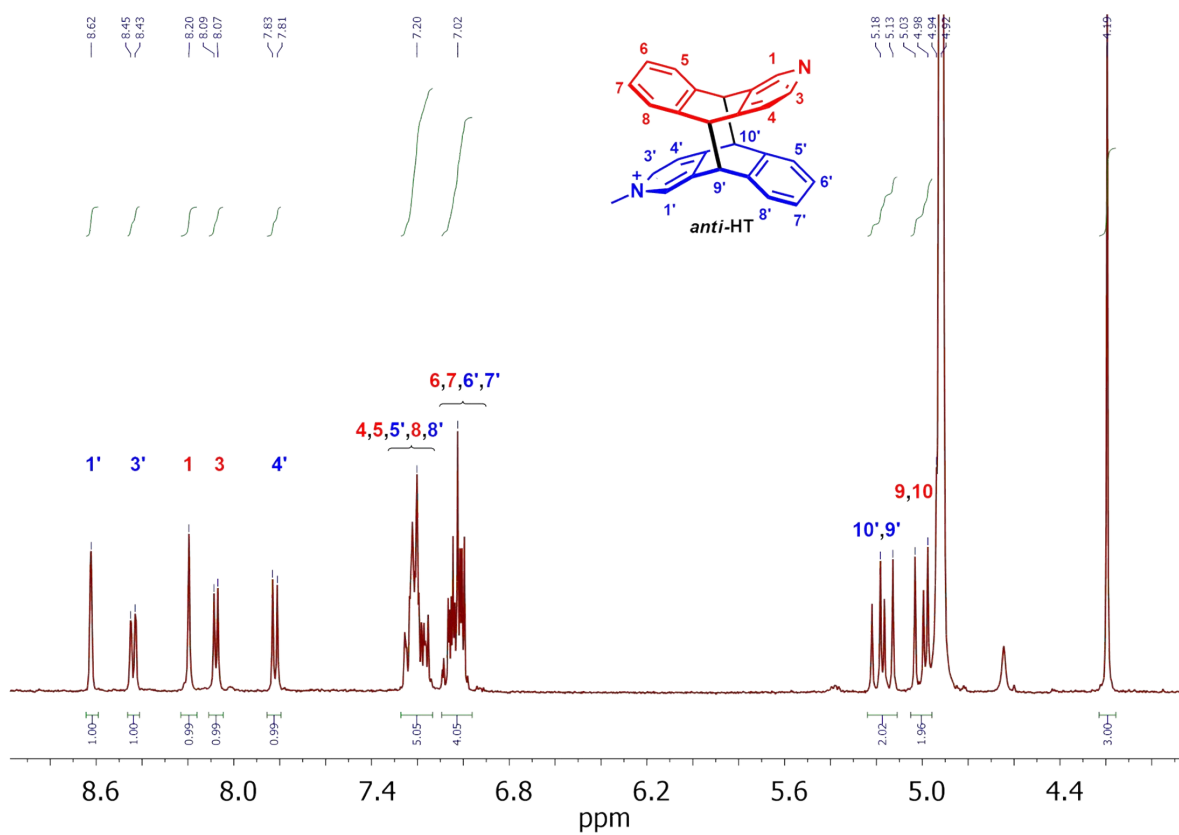
Fig. S26. ^{1}H spectrum of *anti*-HT mixdimer **AM** in methanol-d_4 after isolation of pure regiomer measured at 300 MHz at 298 K.
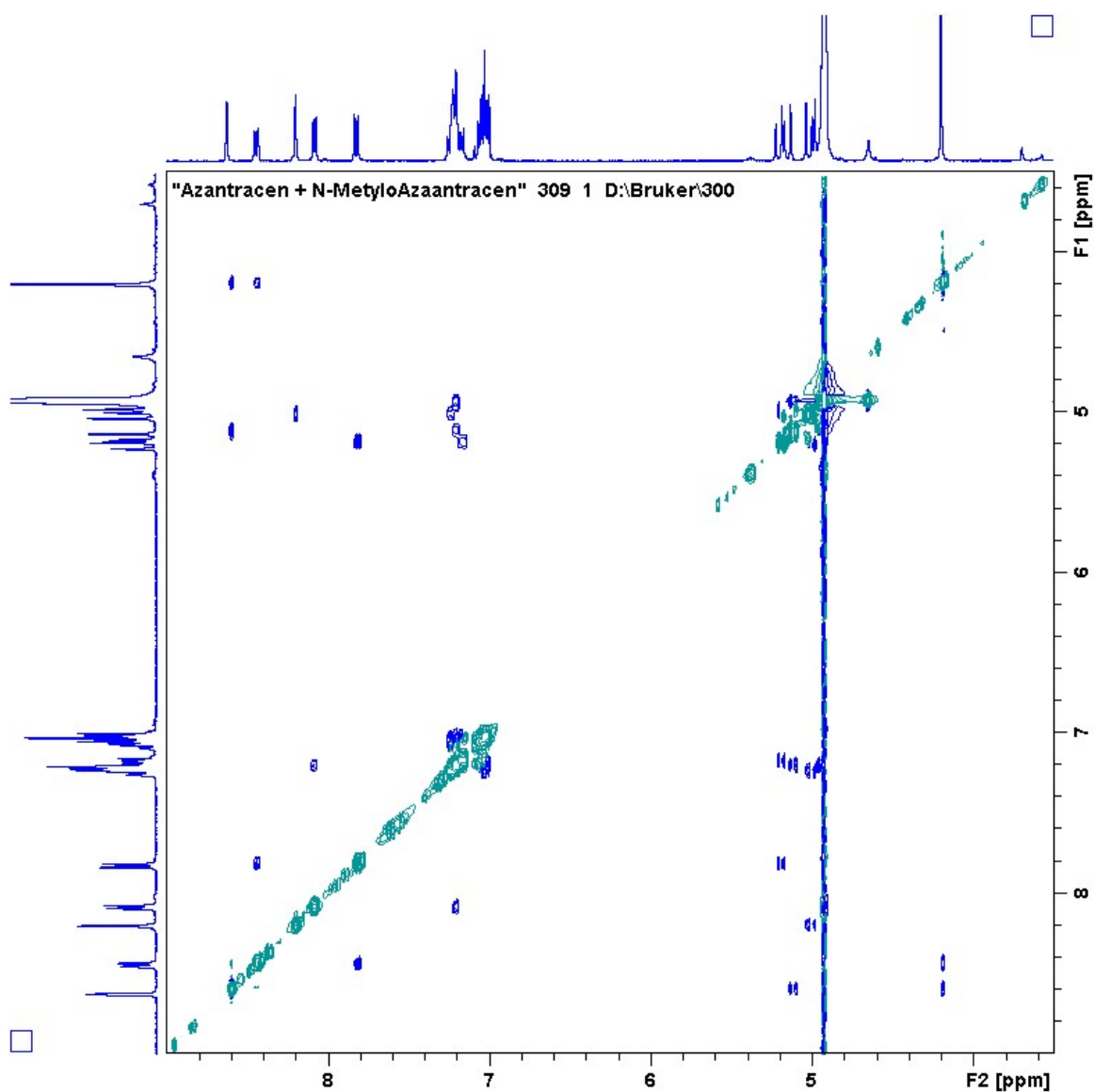
Fig. S27. ^{1}H-^{1}H NOESY spectrum of *anti*-HT mixdimer **AM** in methanol-d_4 after isolation of pure regiomer measured at 300 MHz at 298 K. Mixing time was 1 s.
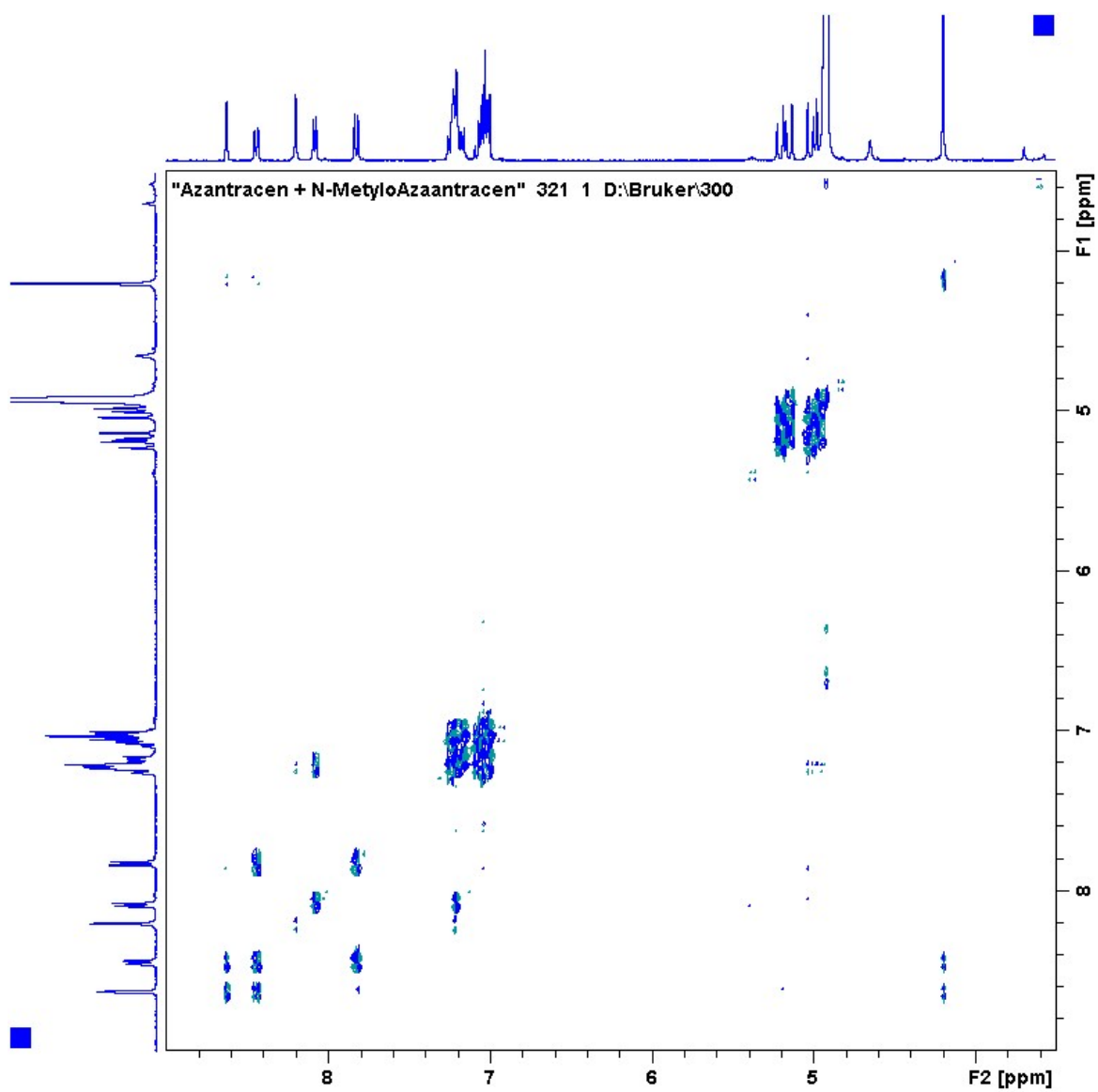
Fig. S28. ^{1}H-^{1}H COSY spectrum of *anti*-HT mixdimer **AM** in methanol-d_4 after isolation of pure regiomer measured at 300 MHz at 298 K.
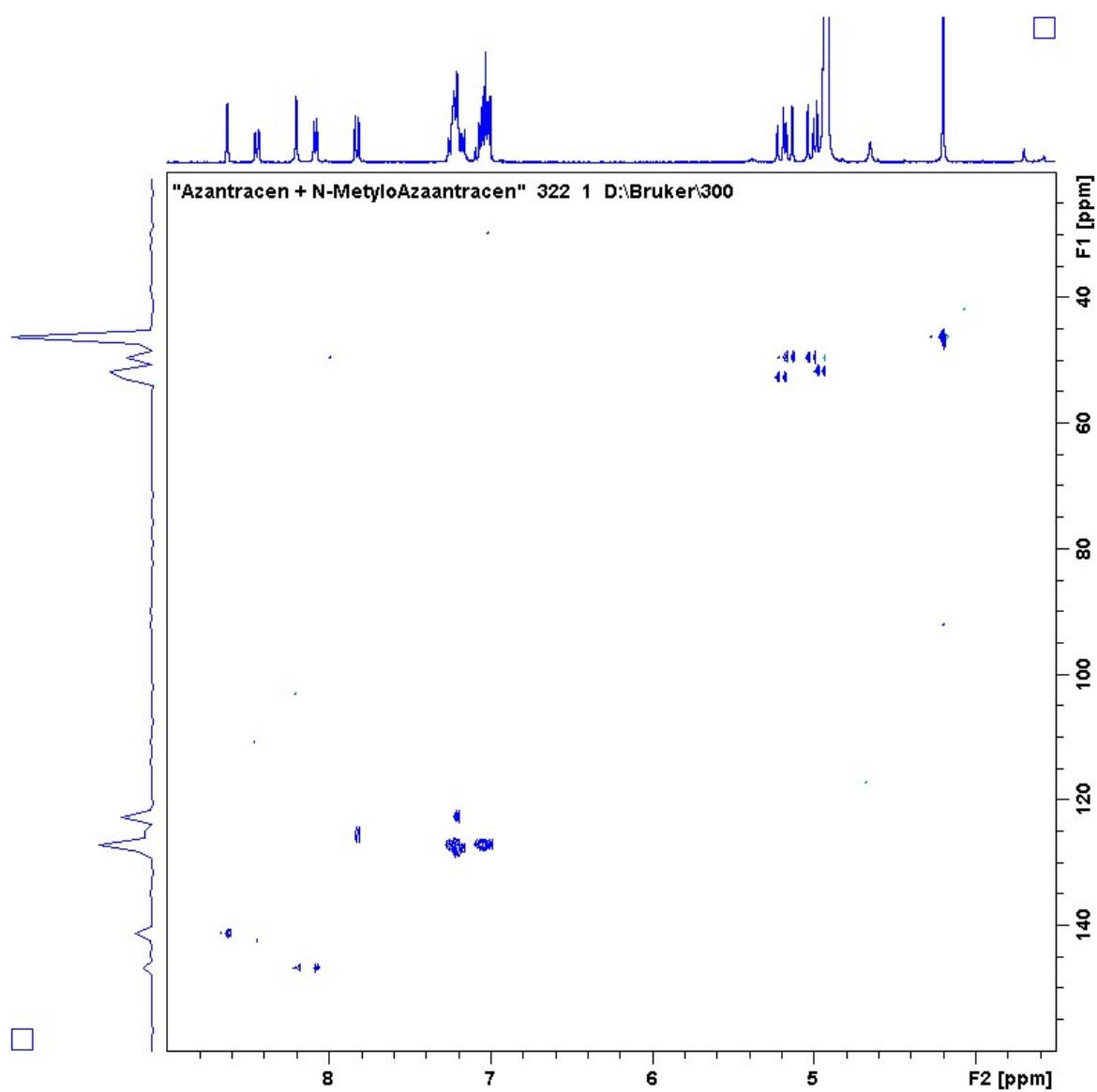
Fig. S29. ^{1}H-^{13}C HSQC spectrum of *anti*-HT mixdimer **AM** in methanol-d_4 after isolation of pure regiomer measured at 300 MHz at 298 K.

3. MS spectra
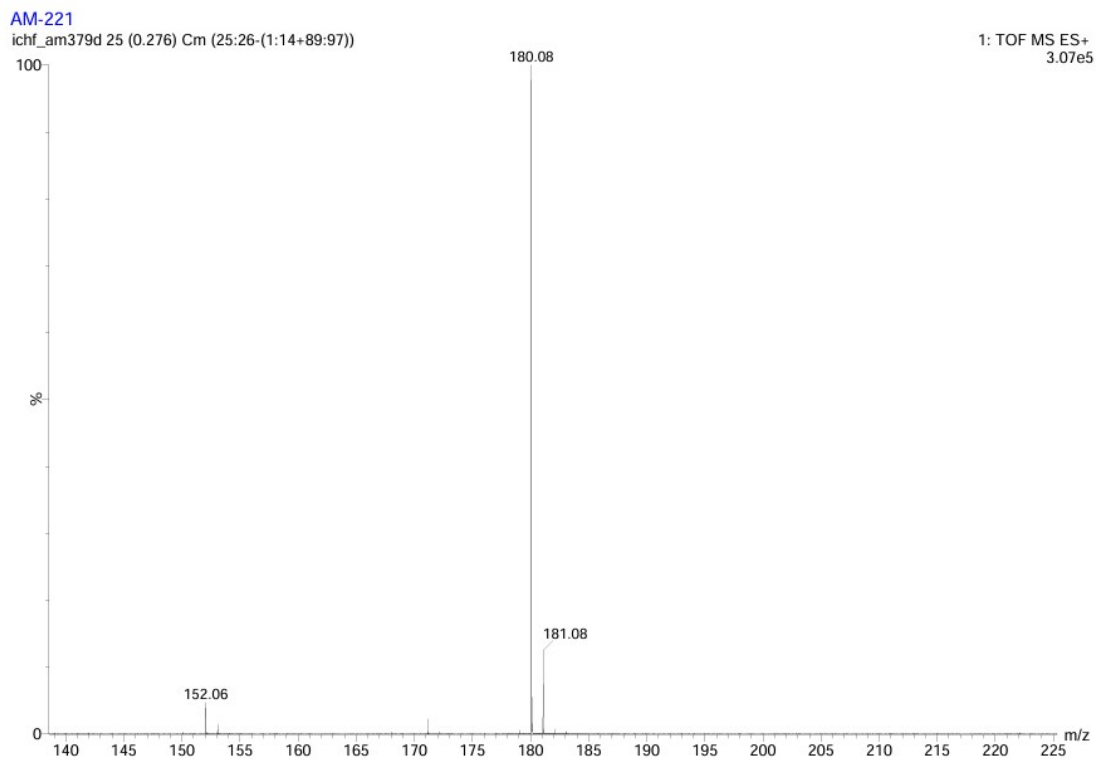
Fig. S30. HR MS spectrum of 2-Azaanthracene (**A**), m/z calcd for [M + H]$^+$ C$_{13}$H$_{10}$N 180.0813, found 180.0818.
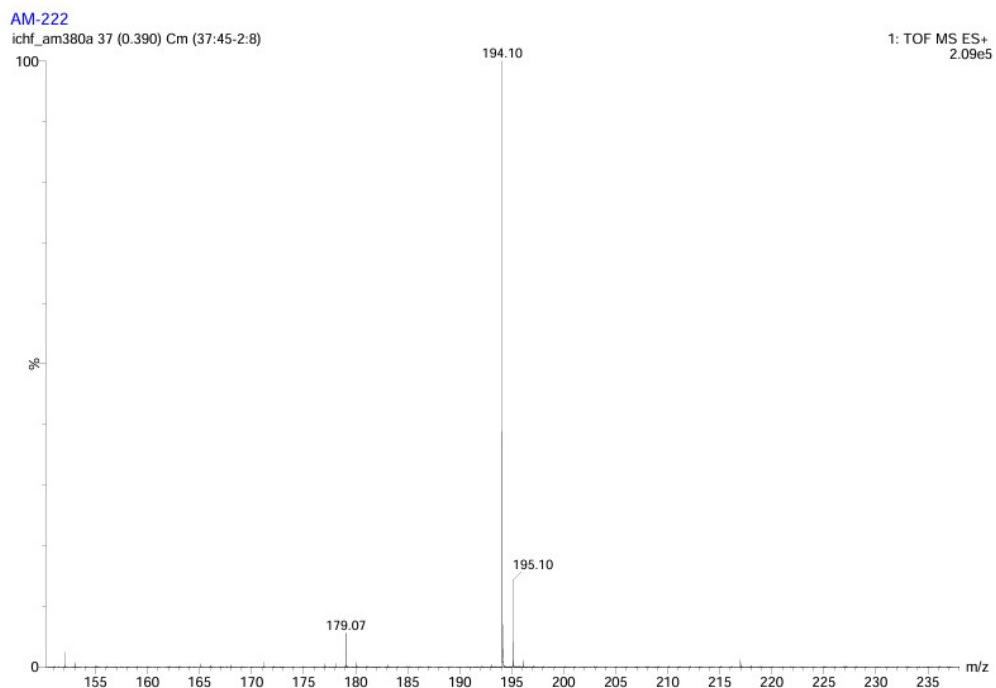
Fig. S31. HR MS spectrum of N-Me-2-azaanthracene (**M**), m/z calcd for [M + H]$^+$ C$_{14}$H$_{12}$N 194.0970, found 194.0972.
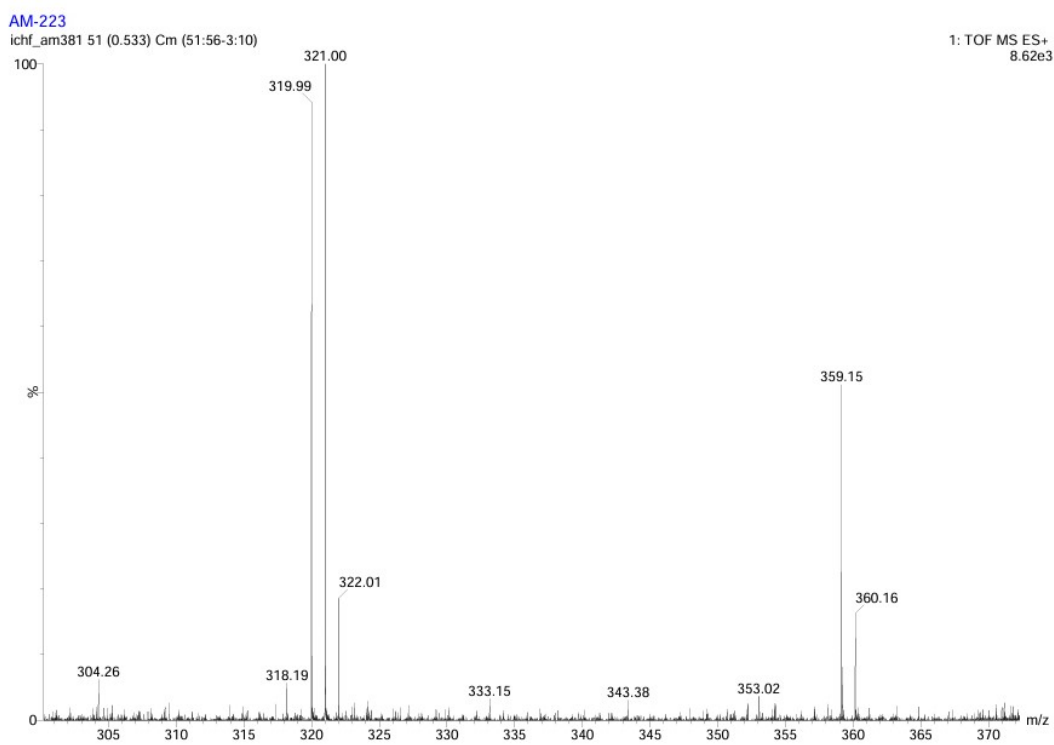
Fig. S32. HR MS spectrum of **AA**, m/z calcd for $[M + H]^+$ $C_{26}H_{19}N_2$ 359.1548, found 359.1544.
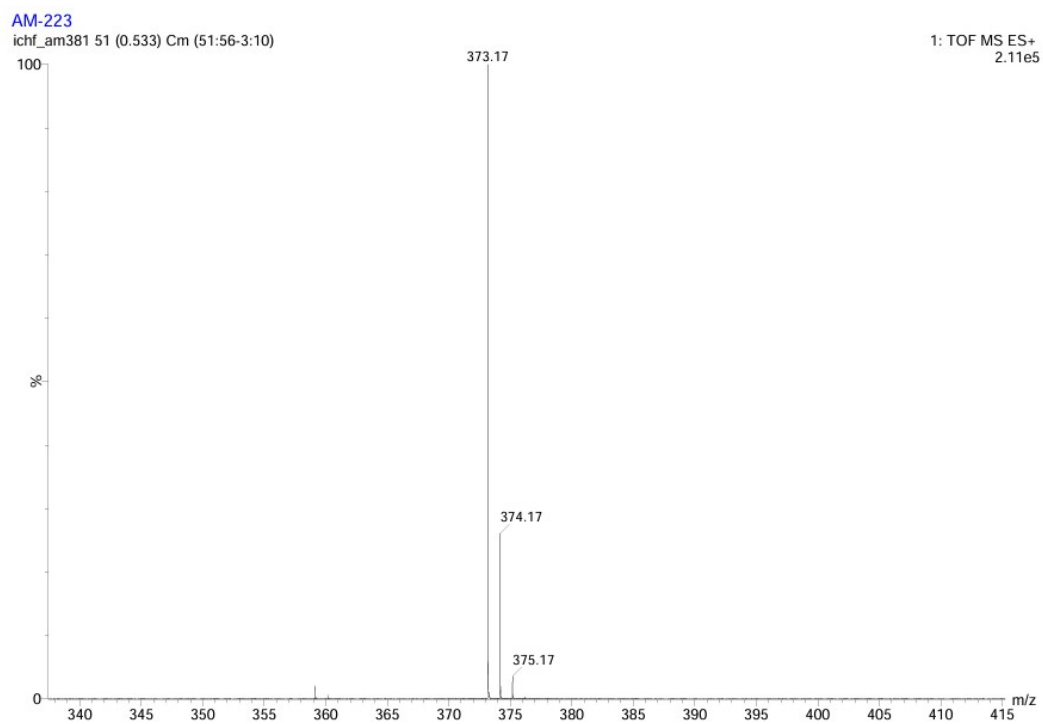
Fig. S33. HR MS spectrum of **AM**, m/z calcd for $[M + H]^+$ $C_{27}H_{21}N_2$ 373.1705, found 373.1708.
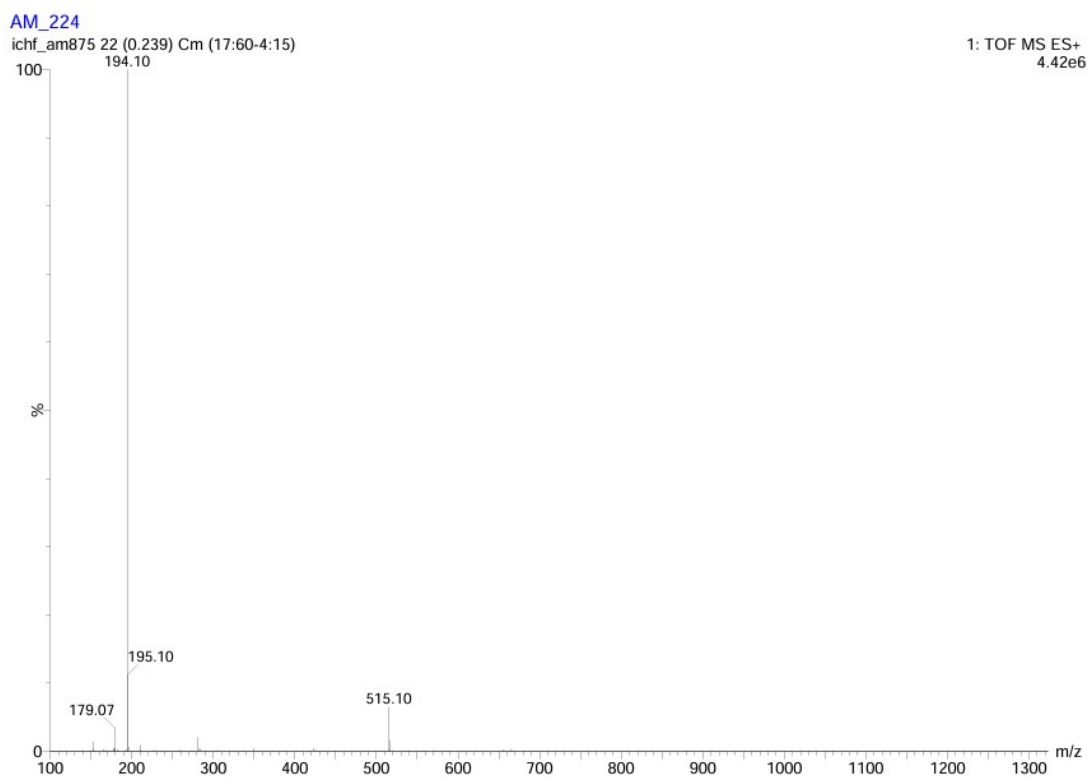
Fig. S34. MS spectrum of **MM**.

4. UV-vis measurements
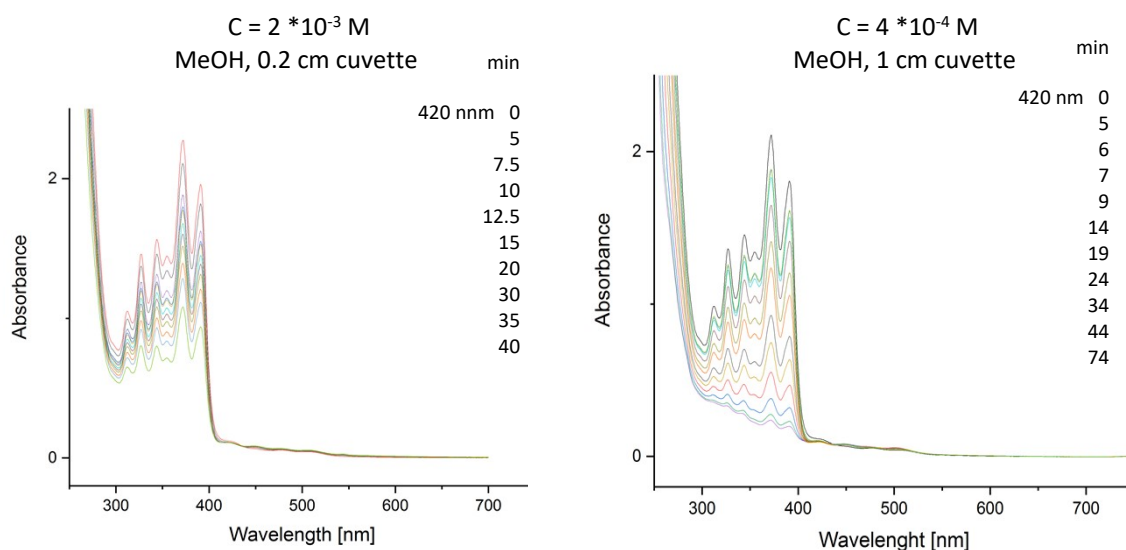
Fig. S35. UV-vis absorption spectra recorded during irradiation of 2-Azaanthracene (**A**) in methanol at 420 nm. The left graph shows results for higher concentration of analyte recorded in 0.2 cm cuvette without stirring, whereas the right graph presents 5 times lower concentration in 1 cm cuvette with stirring. In the right graph, additional irradiation at 365 nm was applied in order to conduct the photodimerization nearly to the end and get an impression about absorption spectrum of the photoproducts.
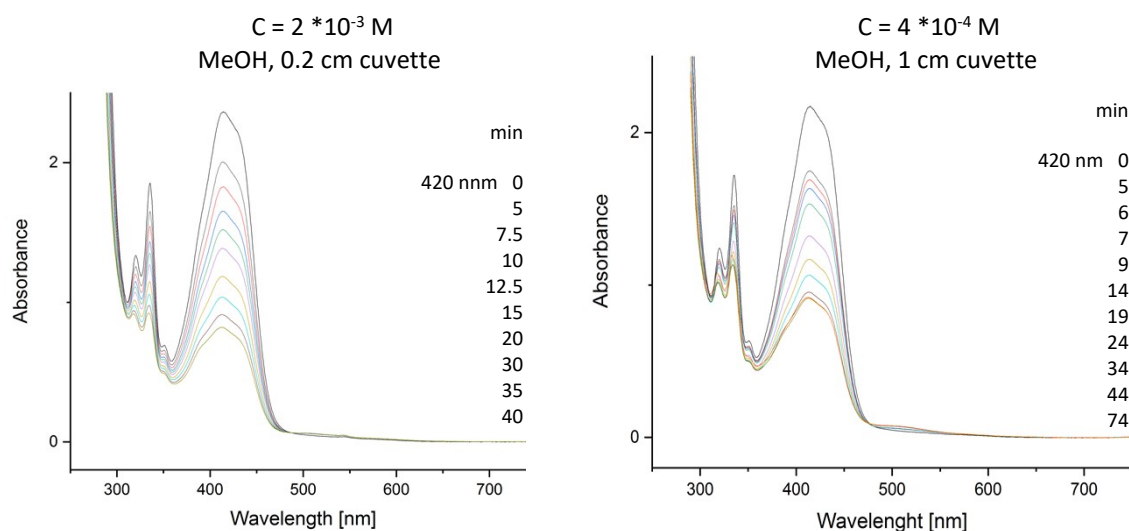
Fig. S36. UV- vis absorption spectra recorded during irradiation of N-methyl-2-azaanthracene (**M**) in methanol at 420 nm. The left graph shows results for higher concentration of analyte recorded in 0.2 cm cuvette without stirring, whereas the right graph presents 5 times lower concentration in 1 cm cuvette with stirring.

5 Photophysics
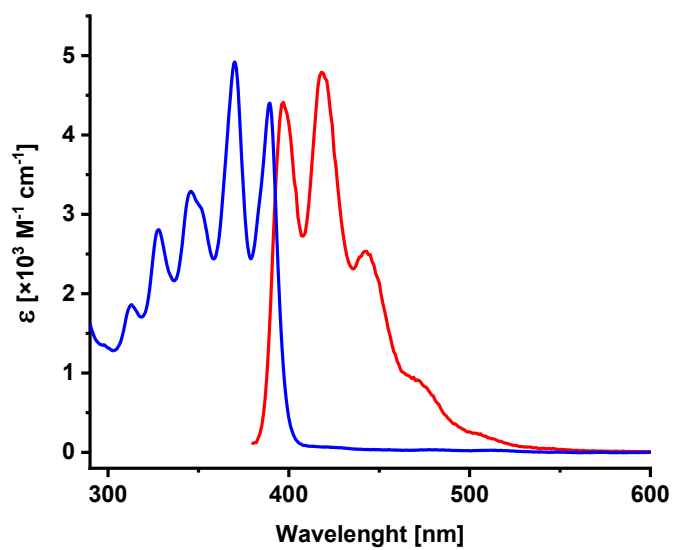
Fig. S37. Absorption and fluorescence spectra of 2-azaanthracene (**A**) in MeOH.
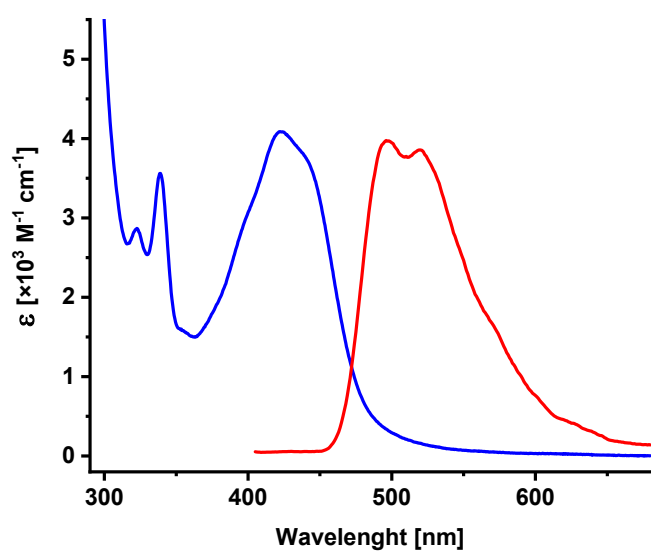
Fig. S38. Absorption and fluorescence spectra of N-methyl-2-azaanthracene (**M**) in MeOH.

Table S1. Photophysical parameters of **A** and **M** in MeOH and DCM.

	Solvent	τ, ns	Φ	$k_r, \times 10^7 s^{-1}$	Φ_Δ
A	MeOH	12.8	0.44	3.4	0.63
A	DCM	13.3	0.48	3.6	0.33
M	MeOH	27.0	0.61	2.3	0.31
M	DCM	26.0	0.10	0.4	0.02

τ- lifetime of fluorescence; Φ - quantum yield of fluorescence; k_r – radiative rate constant;

Φ_Δ - quantum yield of singlet oxygen generation.

Error in the estimation of quantum yield of singlet oxygen generation is 15%.

Error in the estimation of quantum yield of fluorescence is 10%.

6. Quantum-chemical calculations

All semi-empirical calculations have been performed with the MNDO99 code (v7 with upgrades),[3] at the ODM2/MRCI-SD level of theory[4–7] in which the ODM2 electronic structure model has been combined with the multi-reference configuration interaction method with single and double excitations. In these calculations the half-electron restricted open-shell Hartree−Fock (HF) formalism[8] was applied in the self-consistent field (SCF) treatment.

The active space in the MRCI calculations included 12 electrons in 12 orbitals for **AA** and **AM** systems, and 10 electrons in 10 orbitals for the **MM** system (for the orbitals plots, please check Table S1). Three configuration state functions were chosen as references for the MRCI treatment: the SCF configuration and the two closed-shell configurations derived therefrom. The MRCI wave function was built by allowing all single and double excitations from these three references within the defined active space.

The DFT calculations have been performed with the Becke 3-parameter-Lee-Yang-Parr (B3LYP) hybrid functional[9,10] with the Grimme empirical dispersion correction[11,12] modified by the Becke-Johnson damping function[13,14], and with use the def2-SVP basis set[15]. The solvent effects have been accounted for with the Polarizable Continuum Model (PCM) in its integral equation formalism variant (IEFPCM) [16–18]. For the excited electronic states, time-dependent density functional theory (TD-DFT) calculations have been performed with the Tamm-Dancoff approximation (TDA).[19] All DFT calculations have been performed with the Gaussian 16 (rev. C.01) suite of programs[20]

In the ab initio minimum energy conical intersection (MECI) benchmark optimization the Complete Active Space Self-Consisted Field (CASSCF)[21,22] method was employed, with the Dunning correlation-consistent double-zeta basis set (cc-pVDZ)[23]

The calculations were state-averaged (SA) with equal weights between the S0 and S1 states. The employed reduced active space, consisting of 4 electrons in 4 orbitals, can be found in Table S4 in the ESI. In this part, we used the BAGEL software.[24,25]

Table S2. Orbital active space employed in ODM2/MRCI-SD calculations for: AM$^+$ (section a), AA (section b), and MM^{2+} (section c), plotted for respective S1 *anti*-hh dimers.

a)

HOMO-5	HOMO-4	HOMO-3	HOMO-2	HOMO-1	HOMO
LUMO	LUMO+1	LUMO+2	LUMO+3	LUMO+4	LUMO+5

b)

HOMO-5	HOMO-4	HOMO-3	HOMO-2	HOMO-1	HOMO
LUMO	LUMO+1	LUMO+2	LUMO+3	LUMO+4	LUMO+5

c)

HOMO-4	HOMO-3	HOMO-2	HOMO-1	HOMO
LUMO	LUMO+1	LUMO+2	LUMO+3	LUMO+4
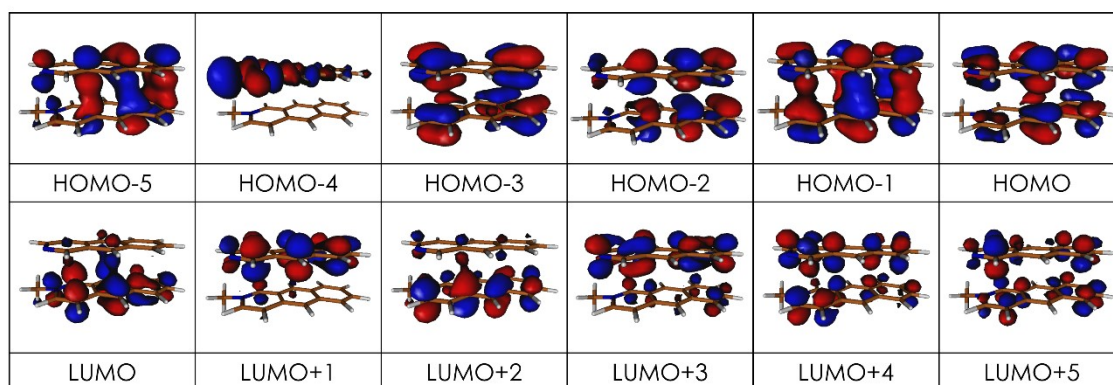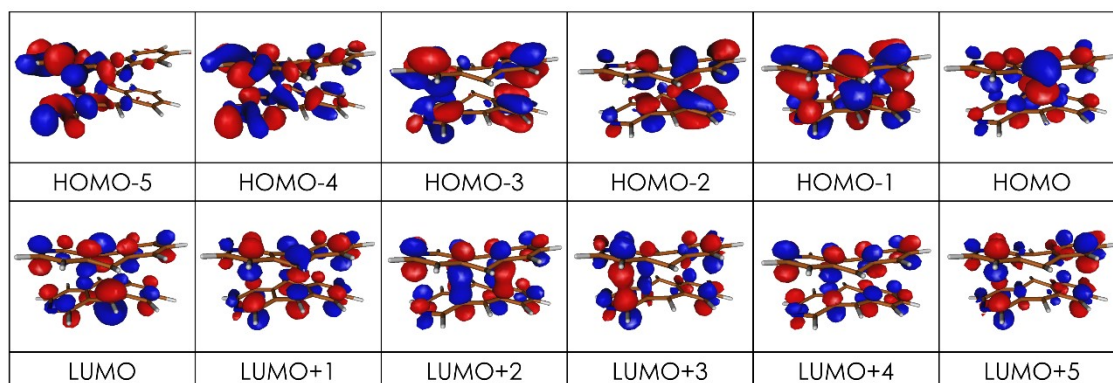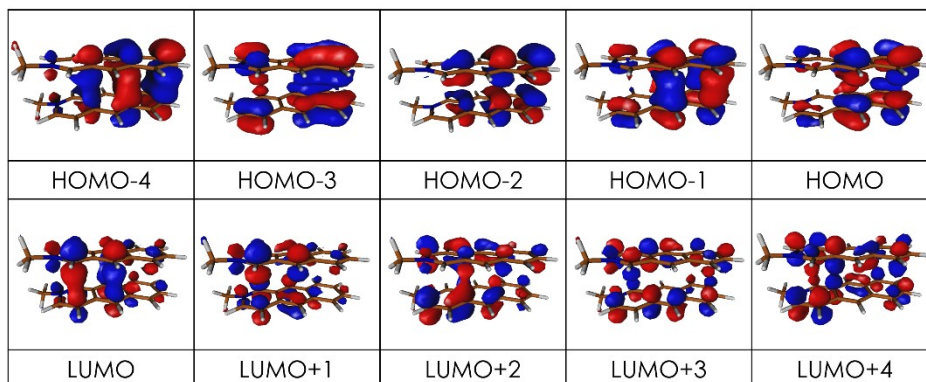
Table S3. Ground-state optimized structures and corresponding energies of **AM** photoproducts (section a) and dimer complexes (section b) obtained at the B3LYP/def2-SVP level of theory, with included GD3-BJ dispersion correction, and solvent effects accounted for at the PCM level (methanol). In all cases the energies are calculated relative to the lowest value for a given type of structure (*i.e.,* the minimum-energy photoproduct or the S0 dimer complex).

a)

anti-hh S_0: 0.015 eV	*anti*-ht S_0: 0.000 eV	*syn*-hh S_0: 0.018 eV	*syn*-ht S_0: 0.001 eV

b)

anti-hh S_0: 0.000 eV	*anti*-ht S_0: 0.048 eV	*syn*-hh S_0: 0.036 eV	*syn*-ht S_0: 0.013 eV
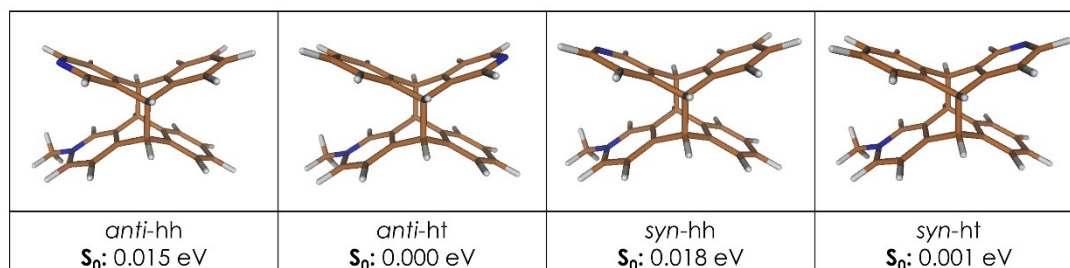
Table S4. Structures of **AM** dimers optimized in the S1 state at the TDA-TDDFT level of theory: B3LYP/def2-SVP with included GD3-BJ dispersion correction, and solvent effects accounted for at the PCM level (methanol). All energies are calculated relative to the lowest-energy S1-regiomer.

anti-hh S_1: 0.00 eV	*anti*-ht S_1: 0.01 eV	*syn*-hh S_1: 0.32 eV	*syn*-ht S_1: 0.02 eV
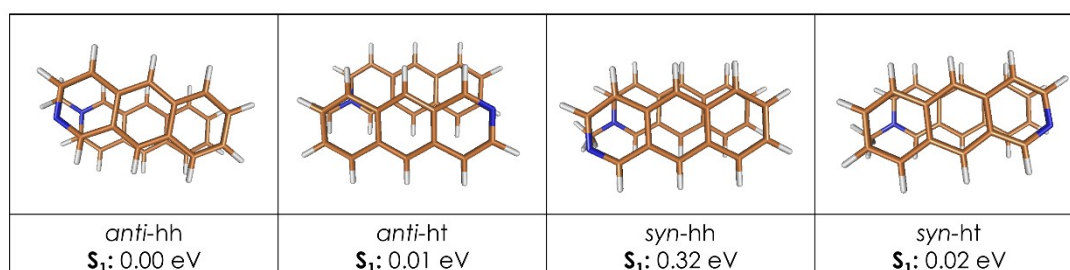
Table S5. Optimized **AM** MECI structures obtained at the CASSCF/cc-pVDZ level of theory (section a), and the orbital active space employed in these calculations (section b), plotted for the respective *anti*-hh regiomer.

a)

anti-hh E_{MECI}: 0.100 eV	*anti*-ht E_{MECI}: 0.000 eV	syn-hh E_{MECI}: 1.066 eV	syn-ht E_{MECI}: 0.778 eV

b)

HOMO-1	HOMO	LUMO	LUMO

Table S6. Optimized **AA** S1 minima (section a) and MECI structures (section b), obtained at the ODM2/MRCI-SD level of theory. The relative energies in the first e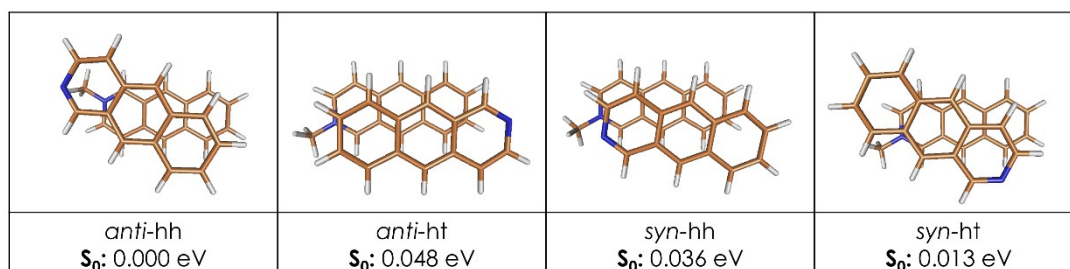xcited state (ΔS_1) are calculated against corresponding values for the *syn*-ht form. The MECI energies (ΔE_{MECI}) are calculated against energies of respective S_1-minima.

a)

AA *anti*-hh ΔS_1 = 0.02 eV	**AA** *anti*-ht ΔS_1 = 0.00 eV	**AA** *syn*-hh ΔS_1 = 0.15 eV	**AA** *syn*-ht ΔS_1 = 0.00 eV

b)

AA *anti*-hh ΔE_{MECI} = 0.07 eV	**AA** *anti*-ht ΔE_{MECI} = 0.10 eV	**AA** *syn*-hh ΔE_{MECI} = 0.24 eV	**AA** *syn*-ht ΔE_{MECI} = 0.28 eV

Table S7. Optimized **MM** S1 minima (section a) and MECI structures (section b), obtained at the ODM2/MRCI-SD level of theory. The relative energies in the first excited state (ΔS_1) are calculated against corresponding values for the *syn*-hh form. The MECI energies (ΔE_{MECI}) are calculated against energies of respective S_1-minima.
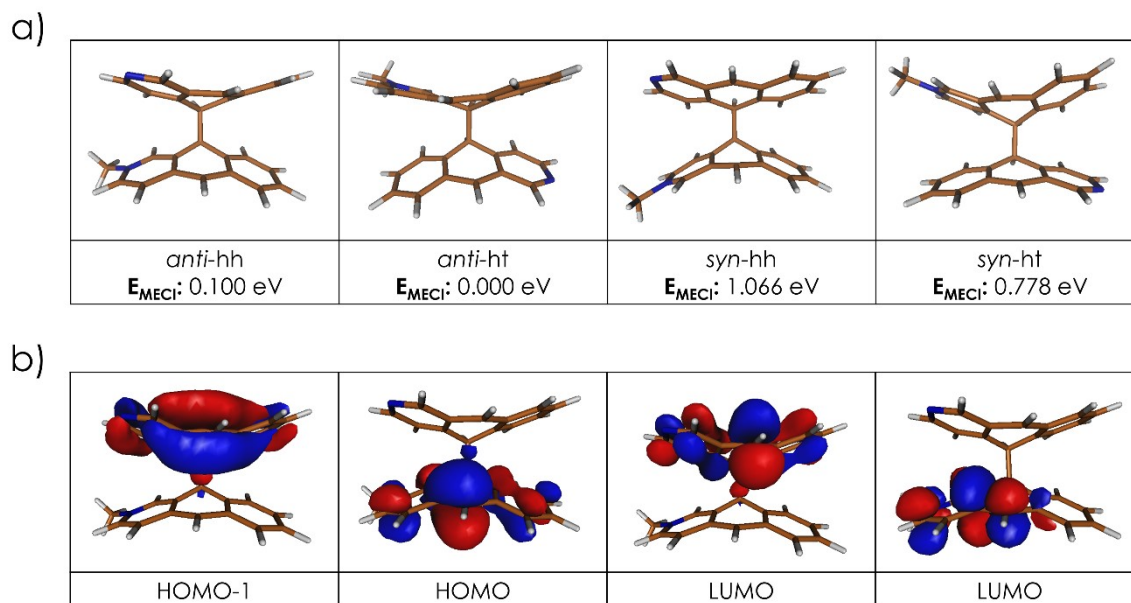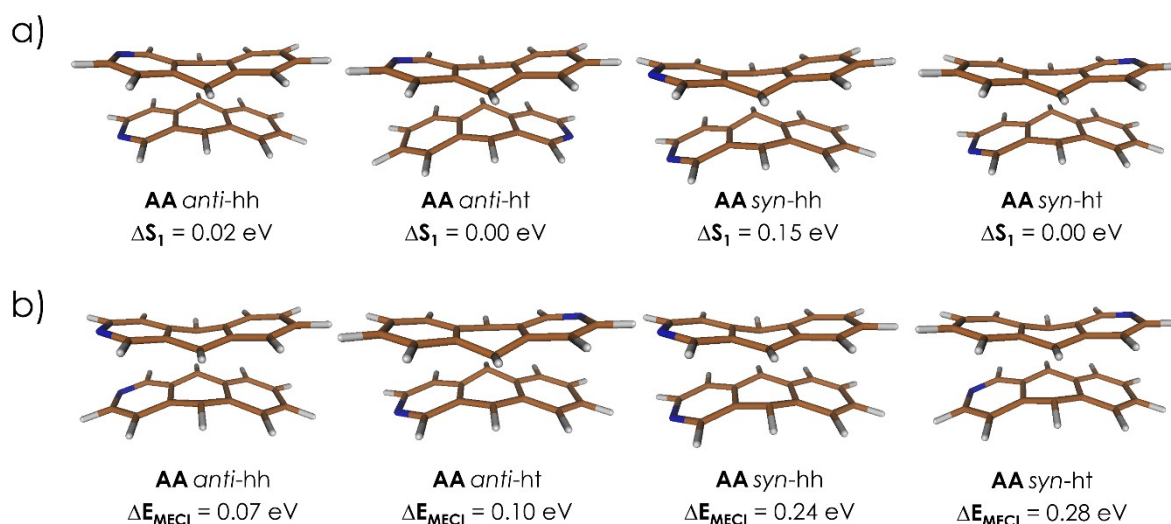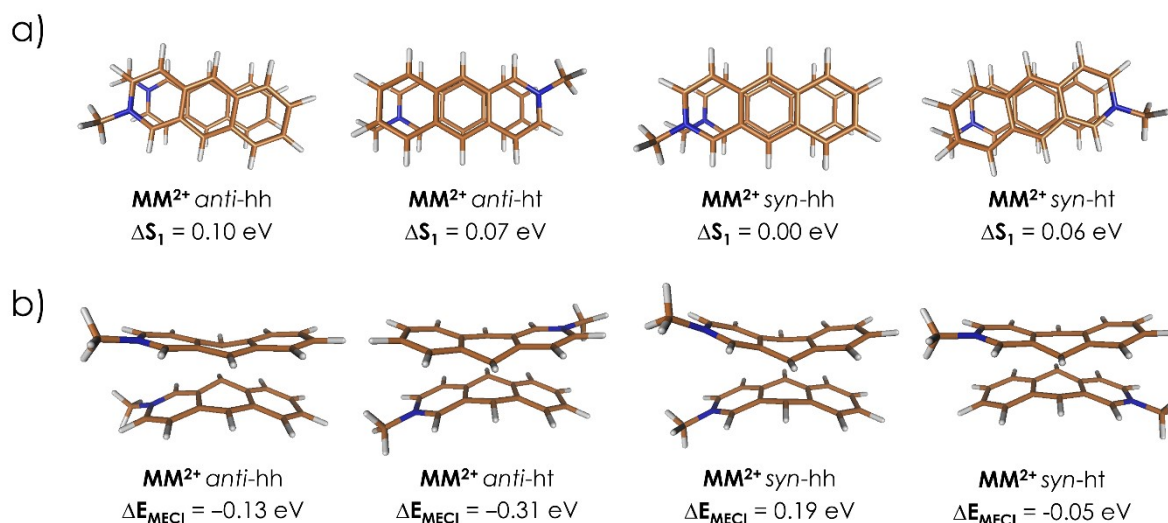
a)

MM^{2+} *anti*-hh
$\Delta S_1 = 0.10$ eV

MM^{2+} *anti*-ht
$\Delta S_1 = 0.07$ eV

MM^{2+} *syn*-hh
$\Delta S_1 = 0.00$ eV

MM^{2+} *syn*-ht
$\Delta S_1 = 0.06$ eV

b)

MM^{2+} *anti*-hh
$\Delta E_{MECI} = -0.13$ eV

MM^{2+} *anti*-ht
$\Delta E_{MECI} = -0.31$ eV

MM^{2+} *syn*-hh
$\Delta E_{MECI} = 0.19$ eV

MM^{2+} *syn*-ht
$\Delta E_{MECI} = -0.05$ eV

7. Literature

1   A. P. Krapcho and T. P. Gilmor, *J. Heterocycl. Chem.*, 1998, **35**, 669–674.

2   J. Ostapko, A. Gorski, J. Buczyńska, B. Golec, K. Nawara, A. Kharchenko, A. Listkowski, M. Ceborska, M. Pietrzak and J. Waluk, *Chem. – A Eur. J.*, 2020, **26**, 16666–16675.

3   W. Thiel, MNDO99 v7.0 with upgrades, Max-Planck-Institut für Kohlenforschung, 2017.

4   P. O. Dral, X. Wu and W. Thiel, *J. Chem. Theory Comput.*, 2019, **15**, 1743–1760.

5   W. Weber and W. Thiel, *Theor. Chem. Acc.*, 2000, **103**, 495–506.

6   A. Koslowski, M. E. Beck and W. Thiel, *J. Comput. Chem.*, 2003, **24**, 714–726.

7   P. O. Dral, X. Wu, L. Spörkel, A. Koslowski, W. Weber, R. Steiger, M. Scholten and W. Thiel, *J. Chem. Theory Comput.*, 2016, **12**, 1082–1096.

8   M. J. S. Dewar, J. A. Hashmall and C. G. Venier, *J. Am. Chem. Soc.*, 1968, **90**, 1953–1957.

9   C. Lee, W. Yang and R. G. Parr, *Phys. Rev. B*, 1988, **37**, 785–789.

10   A. D. Becke, *J. Chem. Phys.*, 1993, **98**, 5648–5652.

11   S. Grimme, *J. Comput. Chem.*, 2004, **25**, 1463–1473.

12   S. Grimme, *J. Comput. Chem.*, 2006, **27**, 1787–1799.

13   S. Grimme, J. Antony, S. Ehrlich and H. Krieg, *J. Chem. Phys.*, 2010, **132**, 154104.

14   S. Grimme, S. Ehrlich and L. Goerigk, *J. Comput. Chem.*, 2011, **32**, 1456–1465.

15   F. Weigend and R. Ahlrichs, *Phys. Chem. Chem. Phys.*, 2005, **7**, 3297–3305.

16   R. Improta, V. Barone, G. Scalmani and M. J. Frisch, *J. Chem. Phys.*, 2006, **125**, 54103.

17   R. Improta, G. Scalmani, M. J. Frisch and V. Barone, *J. Chem. Phys.*, 2007, **127**, 74504.

18   G. Scalmani, M. J. Frisch, B. Mennucci, J. Tomasi, R. Cammi and V. Barone, *J. Chem. Phys.*, 2006, **124**, 94107.

19   S. Hirata and M. Head-Gordon, *Chem. Phys. Lett.*, 1999, **314**, 291–299.

20   Gaussian 16, Revision C.01, M. J. Frisch, G. W. Trucks, H. B. Schlegel, G. E. Scuseria, M. A. Robb, J. R. Cheeseman, G. Scalmani, V. Barone, G. A. Petersson, H. Nakatsuji, X. Li, M. Caricato, A. V. Marenich, J. Bloino, B. G. Janesko, R. Gomperts, B. Mennucci, H. P. Hratchian, J. V. Ortiz, A. F. Izmaylov, J. L. Sonnenberg, D. Williams-Young, F. Ding, F. Lipparini, F. Egidi, J. Goings, B. Peng, A. Petrone, T. Henderson, D. Ranasinghe, V. G. Zakrzewski, J. Gao, N. Rega, G. Zheng, W. Liang, M. Hada, M. Ehara, K. Toyota, R. Fukuda, J. Hasegawa, M. Ishida, T. Nakajima, Y. Honda, O. Kitao, H. Nakai, T. Vreven, K. Throssell, J. A. Montgomery, Jr., J. E. Peralta, F. Ogliaro, M. J. Bearpark, J. J. Heyd, E. N. Brothers, K. N. Kudin, V. N. Staroverov, T. A. Keith, R. Kobayashi, J. Normand, K. Raghavachari, A. P. Rendell, J. C. Burant, S. S. Iyengar, J. Tomasi, M. Cossi, J. M. Millam, M. Klene, C. Adamo, R. Cammi, J. W. Ochterski, R. L. Martin, K. Morokuma, O. Farkas, J. B. Foresman, and D. J. Fox, Gaussian, Inc., Wallingford CT, 2019.

21   B. O. Roos, *Int. J. Quantum Chem.*, 1980, **18**, 175–189.

22   B. O. Roos, P. R. Taylor and P. E. M. Sigbahn, *Chem. Phys.*, 1980, **48**, 157–173.

23   T. H. Dunning Jr., *J. Chem. Phys.*, 1989, **90**, 1007–1023.

24   BAGEL, Brilliantly Advanced General Electronic-structure Library. http://www.nubakery.org under the GNU General Public License.

25   T. Shiozaki, *WIREs Comput. Mol. Sci.*, 2018, **8**, e1331–e1331.